## High-order post-Newtonian expansion of the generalized redshift invariant for eccentric-orbit, equatorial extreme-mass-ratio inspirals with a spinning primary

#### Christopher Munna

Department of Physics and Astronomy, University of North Carolina, Chapel Hill, North Carolina 27599, USA and MIT Kavli Institute, Massachusetts Institute of Technology, Cambridge, Massachusetts 02139, USA

(Received 27 July 2023; accepted 14 September 2023; published 10 October 2023)

We derive new terms in the post-Newtonian (PN) expansion of the generalized redshift invariant  $\langle u^t \rangle_{\tau}$  for a small body in eccentric, equatorial orbit about a massive Kerr black hole. The series is computed analytically using the Teukolsky formalism for first-order black hole perturbation theory, along with the Chrzanowski, Cohen, Kegeles method for metric reconstruction using the Hertz potential in ingoing radiation gauge. Modal contributions with small values of l are derived via the semianalytic solution of Mano-Suzuki-Takasugi, while the remaining values of l to infinity are determined via direct expansion of the Teukolsky equation. Each PN order is calculated as a series in eccentricity e but kept exact in the primary black hole's spin parameter a. In total, the PN terms are expanded to  $e^{16}$  through 6PN relative order, and separately to  $e^{10}$  through 8PN relative order. Upon grouping eccentricity coefficients by spin dependence, we find that many resulting component terms can be simplified to closed-form functions of eccentricity, in close analogy to corresponding terms derived previously in the Schwarzschild limit. We use numerical calculations to compare convergence of the full series to its Schwarzschild counterpart and discuss implications for gravitational wave analysis.

#### DOI: 10.1103/PhysRevD.108.084012

#### I. INTRODUCTION

The radiative dynamics of binary black hole inspirals with an extreme mass ratio (that is, extreme-mass-ratio inspirals, or EMRIs) continues to be an active area of research. Theoretical models must be able to predict the entire trajectories of these inspirals to within a fraction of a radian over their lifetimes to produce accurate waveform templates for the coming space-based gravitational wave detector, LISA [1].

Over the past several years, we have sought to advance knowledge of EMRI motion and radiation through high-order post-Newtonian (PN) approximations to first-order black hole perturbation theory (BHPT) [2]. Analysis of first-order BHPT in the PN regime has a long and rich history, with a 1PN expression for the radiation first derived for nearly circular inspirals in 1980 [3]. This was later extended by a series of results in the 1990s [4–8], which also typically focused on circular or nearly circular orbits. A full review of the early history of these efforts can be found in [9]. Eventually, an analytic PN expansion of the energy flux for circular EMRIs on a Schwarzschild background was derived all the way to 22PN order [10]. The author of that paper discovered that the expansion's fidelity to numerical data near the strong-field regime continued to

improve to the highest order, supporting the utility of very deep PN series.

Inspired by these results, we first studied the case of eccentric-orbit inspirals on a Schwarzschild background, which had previously seen much less development, using the Mano-Suzuki-Takasugi (MST) solutions to the Regge-Wheeler-Zerilli (RWZ) equations [11–14]. With an implementation of this formalism in *Mathematica*, we derived several notable features of the orbital evolution. We first determined the (energy and angular momentum) fluxes at infinity to 19PN, with each term expanded in eccentricity to  $e^{10}$ , as well as to 10PN and  $e^{20}$  [15–18]. This effort was then extended to the horizon fluxes, which were computed to 18PN (relative order)/ $e^{10}$  and  $10PN/e^{20}$  [2,19].

It later proved possible to use this code to derive PN series for local gauge-invariant corrections to the conservative motion, including the redshift invariant (expanded to  $10\text{PN}/e^{20}$  [20]) and the spin-precession invariant (expanded to  $9\text{PN}/e^{16}$  [21]). These series are also valuable to high orders, as conservative-sector expansions can be used to inform the effective-one-body (EOB) formalism, which accurately describes binary dynamics across vast regions of parameter space [22–32]. In general, the conservative motion contributes to the inspiral's evolution at first

postadiabatic order, a level necessary for parameter estimation with LISA [1].

As most astrophysical black holes have nonzero spin, it is necessary to understand the corresponding dynamics for EMRIs with a central Kerr black hole. Early efforts to analyze the spinning case in the PN regime began in the 1990s [33–36], typically restricting to the nearly circular, nearly equatorial case. Over time these approaches were refined, and the energy flux for circular equatorial inspirals was more recently derived to 11PN for arbitrary spin [37]. As before, we seek to derive comparable results for eccentric-orbit binaries, which have historically been underdeveloped in comparison. As an intermediate step to fully generic inspirals, we first restrict our efforts to the case of equatorial eccentric orbits. Fortunately, many of the theoretical and computational techniques used to expand the MST-RWZ formalism mentioned above can be translated to the related (but more complicated) MST-Teukolsky formalism for perturbations about a Kerr background [14,38,39]. We recently used this approach to derive series for the fluxes at infinity to 8PN and  $e^{20}$  [40]. Along the way we discovered that many of the eccentricity series could be manipulated into exact (closed-form) functions. The energy and angular momentum absorbed by the central black hole has been found to a similar level, and those results will be published in a future paper [41].

As in the Schwarzschild case, we are now equipped to analyze the conservative sector of the first-order motion. The most well-known quantity characterizing the conservative sector is the redshift invariant  $u^t$ , which was first defined for circular Schwarzschild orbits and derived using the full PN theory to 3PN order by Detweiler [42] (see [43] for a review of PN theory). As the significance of the redshift invariant in encoding the conservative dynamics became more widely appreciated, researchers began to derive deeper PN expansions in the small-mass-ratio limit using BHPT [44,45], and this process was eventually carried out to 21.5PN [46].

The extension to eccentric Schwarzschild orbits was first described by Barack and Sago [47], who defined the so-called generalized redshift invariant  $\langle u^t \rangle_{\tau}$  as the propertime average of  $u^t$  over one radial libration. The generalized redshift invariant was later derived to 3PN order in [48] using the full PN theory and then subsequently higher order for EMRIs using BHPT [25,27,31,32]. The most recent development was an expansion to 10PN and  $e^{20}$ , with many PN terms found to yield closed-form functions of eccentricity [20]. That work also presented a set of curious connections between the (conservative-sector) redshift expansion and the (dissipative-sector) energy flux expansion, in that the two series share identical leading logarithm terms (see [15,17,20] for additional details).

Because of its added difficulty, the redshift invariant for EMRIs with a Kerr primary has seen less progress, being first computed for circular equatorial EMRIs in 2012 [49].

A BHPT-PN expansion was derived several years later to 8.5PN order [50], with each PN term expanded in spin to  $a^4$ . An 8.5PN series remaining exact in spin was then found in the work [51]. The eccentric, equatorial case was calculated numerically as part of a larger metric reconstruction effort in [52]. Then, the corresponding BHPT-PN expansion was derived in the small-e, small-a limit to 8.5PN/ $\mathcal{O}(e^2)/\mathcal{O}(a^2)$  in [53] and then to 8.5PN/ $\mathcal{O}(e^4)/\mathcal{O}(a^2)$  in [54]. The work [54] also produced a low-order derivation of the redshift within the full PN theory for spinning bodies, using that result to confirm the first few terms in their BHPT-PN calculation.

The present effort now seeks to extend this calculation beyond the nearly circular, nearly Schwarzschild regime by deriving results that are exact in a and high order in e. Specifically, we show series to 6PN and  $e^{16}$  and to 8PN and  $e^{10}$ , both remaining exact in a. To the author's knowledge, this is the first expansion of the redshift for eccentric orbits on a Kerr background with terms exact in a. We assess the convergence of this series by comparing to numerical calculations for combinations from the sets  $p \in \{10, 20\}$ ,  $e \in \{1/10, 1/5\}, a \in \{1/4, 1/2, 9/10\}$  for semilatus rectum p. We find that convergence weakens with increasing a and e, but that the full expansion is accurate to better than one part in 10<sup>4</sup> for most of these orbits. This calculation will serve as a final intermediate step on the path to generic (eccentric/inclined) inspirals on a Kerr background, which has not yet been computed analytically or numerically (though the numerical infrastructure for generic orbits does now exist [55]).

Calculation of the redshift invariant requires the local regularized metric perturbation, which can be found via the Chrzanowski, Cohen, Kegeles (CCK) metric reconstruction procedure [56–59]. We use the MST-Teukolsky solutions to form the Hertz potential and then apply a sequence of linear operations to produce components of the perturbed metric at the location of the smaller body in ingoing radiation gauge. We find that, as in the Schwarzschild case, the leading PN order of each l mode is constant in l, necessitating PN series for all l. This difficulty is resolved using a PN ansatz solution for large l that is general in l[44,46,51]. Thus, we use the MST solutions for small  $l \ge 2$ and the ansatz for large l, along with a separate metric completion procedure for l = 0 and l = 1. This general-lansatz solution can also be expanded about  $l = \infty$  to determine the divergent behavior of the summation and then regularize each l mode of the full solution. In total the process is relatively similar to that for eccentric Schwarzschild EMRIs, though the introduction of the spin parameter a and loss of spherical symmetry add several technical hurdles and greatly increase the computational complexity.

The structure of this paper is as follows. In Sec. II we briefly outline the problem setup for first-order BHPT on a Kerr background and the Teukolsky-MST formalism in the

PN limit. We then discuss how to apply the (PN-expanded) MST solutions to the CCK procedure for metric reconstruction using the Hertz potential, as the local metric perturbation is the primary constituent of the redshift invariant. Section III details the derivation of metric perturbation expansions for general l, with emphasis on the unique theoretical and computational challenges contained therein. In Sec. IV we briefly review the metric completion piece and our chosen regularization scheme for the redshift invariant. Section V then details the explicit expansion results to 6PN/e<sup>16</sup> and 8PN/e<sup>10</sup>, which are also posted in multiple online repositories [60,61]. Multiple new closed-form expressions are found, and the structure of the expansion's spin dependence is discussed, as well as its convergence against numerical data. Section VI concludes with a summary and an outlook.

Throughout this paper we apply the metric signature (-+++) and primarily choose units such that c=G=1, though we frequently retain powers of  $\eta=1/c$  to track PN order. Our notation for the Teukolsky and MST formalisms follows that found in [39,51].

# II. REVIEW OF THE TEUKOLSKY AND MST FORMALISMS

We briefly review the background and setup for first-order perturbations about a Kerr background caused by a small mass in equatorial orbit. At each step we seek expressions that are suitable for expansion in the PN limit, whether through the direct parameter  $\eta = 1/c$  or through a measure of orbital separation such as 1/p for semilatus rectum p. These methods are more extensively detailed in [18,40], based on earlier Kerr work in [50,51,53,54] and Schwarzschild work in [27,44–46,62].

#### A. Bound equatorial orbits on a Kerr background

At lowest order, the secondary is treated as a point mass  $\mu$  in bound geodesic orbit about a Kerr black hole of mass M with  $\varepsilon = \mu/M \ll 1$ . The line element in Boyer-Lindquist coordinates  $x^{\mu} = \{t, r, \theta, \varphi\}$  is

$$ds^{2} = -\left(1 - \frac{2Mr}{\Sigma}\right)dt^{2} - \frac{4Mar\sin^{2}\theta}{\Sigma}dtd\varphi + \frac{\Sigma}{\Delta}dr^{2} + \Sigma d\theta^{2} + \left(r^{2} + a^{2} + \frac{2Ma^{2}r\sin^{2}\theta}{\Sigma}\right)\sin^{2}\theta d\varphi^{2},$$
(2.1)

where  $\Sigma = r^2 + a^2 \cos^2 \theta$ ,  $\Delta = r^2 - 2Mr + a^2$ , and a is the spin of the primary.

We now restrict the orbit to the equatorial plane, which leads to the following equations of motion:

$$\begin{pmatrix} r^2 \frac{dt}{d\tau} \end{pmatrix} = (a\mathcal{L} - a^2 \mathcal{E}) + \frac{r^2 + a^2}{\Delta} (\mathcal{E}(r^2 + a^2) - a\mathcal{L}), 
\begin{pmatrix} r^2 \frac{dr}{d\tau} \end{pmatrix}^2 = [\mathcal{E}(r^2 + a^2) - a\mathcal{L}]^2 - \Delta[(a\mathcal{E} - \mathcal{L})^2 + r^2], 
\begin{pmatrix} r^2 \frac{d\varphi}{d\tau} \end{pmatrix} = \mathcal{L} - a\mathcal{E} + \frac{a}{\Delta} (\mathcal{E}(r^2 + a^2) - a\mathcal{L}).$$
(2.2)

Here  $\mathcal{E}$  is the (conserved) specific energy and  $\mathcal{L}$  the specific angular momentum. As noted in [40], these equations of motion are only dependent on the radial coordinate  $r(\tau)$ . This implies that we do not have to invoke the use of Mino time  $d\lambda = d\tau/\Sigma$  and can instead move immediately to the Darwin parametrization. As is typical for Schwarzschild geodesics, we describe the motion in terms of the set  $\{\chi, p, e\}$  for relativistic anomaly  $\chi$ , semilatus rectum p, and eccentricity e [63–65], with

$$r_p(\chi) = \frac{pM}{1 + e\cos\chi}. (2.3)$$

One radial libration occurs with each  $2\pi$  advance in  $\chi$ . Then, defining  $\tilde{a} = a/M$  and  $\hat{\mathcal{L}} = \mathcal{L}/M - \tilde{a}\mathcal{E}$ , we find the following relations [66]:

$$\mathcal{E}^{2} = \frac{(1 - e^{2})^{2}}{p^{3}} \hat{\mathcal{L}}^{2} + 1 - \frac{1 - e^{2}}{p},$$

$$\mathcal{E} = -\frac{p - 3 - e^{2}}{2\tilde{a}p} \hat{\mathcal{L}} - \frac{\tilde{a}^{2} - p}{2\tilde{a}\hat{\mathcal{L}}}.$$
(2.4)

These equations can be solved exactly for  $\mathcal{E}(p,\tilde{a},e)$  and  $\hat{\mathcal{L}}(p,\tilde{a},e)$ , though the results are lengthy (they are given in [40]). However, we note that 1/p is a standard PN parameter, in which  $\mathcal{E}$  and  $\hat{\mathcal{L}}$  can be easily expanded. To simplify the process somewhat, we define  $v=1/\sqrt{p}$  and compute series about v=0. Then, just as in the Schwarzschild case, we expand each PN order in e to prepare for the eventual source integration. On the other hand, we make no approximations with respect to a, leaving each step in the expansion process exact in that parameter.

Applying these definitions and relations into the equations (2.2) leads to the following ordinary differential equations (ODEs) for the coordinates:

$$\frac{d\tau}{d\chi} = \frac{M}{v^{3}(1 + e\cos(\chi))^{2}\sqrt{1 + \hat{\mathcal{L}}^{2}v^{4}(e^{2} - 2e\cos\chi - 3)}}$$

$$\frac{dt}{d\chi} = \left(\frac{d\tau}{d\chi}\right) \frac{\mathcal{E} + \mathcal{E}\tilde{a}^{2}v^{4}(1 + e\cos\chi)^{2} - 2\tilde{a}v^{6}\hat{\mathcal{L}}(1 + e\cos\chi)^{3}}{1 - 2v^{2}(1 + e\cos\chi) + \tilde{a}^{2}v^{4}(1 + e\cos\chi)^{2}}$$

$$\frac{d\varphi}{d\chi} = \frac{v[\mathcal{L} - 2v^{2}\hat{\mathcal{L}}(1 + e\cos\chi)]}{[1 - 2v^{2}(1 + e\cos\chi) + \tilde{a}^{2}v^{4}(1 + e\cos\chi)^{2}]\sqrt{1 + \hat{\mathcal{L}}^{2}v^{4}(e^{2} - 2e\cos\chi - 3)}}.$$
(2.5)

These equations are then readily PN expanded in v and e, and the result is trivially integrated to yield expansions for  $t(\chi)$  and  $\varphi(\chi)$ . They can also be solved exactly using elliptic integrals [67]. Then, the radial period is given by  $T_r = t(2\pi)$ , the radial frequency by  $\Omega_r = 2\pi/T_r$ , and the azimuthal frequency by  $\varphi(2\pi)/T_r$ .

#### B. The Teukolsky master equations

Bound motion acts as a periodic source for the first-order gravitational perturbations. On a Kerr background these can be encoded by a set of Teukolsky master functions  ${}_{s}R_{lm\omega}$  in radiation gauge [38,39] and associated spin-weighted spheroidal harmonics  ${}_{s}S_{lm\omega}$ . We will focus on the functions with spin-weight s=-2, which are governed by the equations,

$$\Delta^{2} \frac{d}{dr} \left( \frac{1}{\Delta} \frac{d_{-2} R_{lm\omega}}{dr} \right) + \left[ \frac{K^{2} + 4i(r - M)K}{\Delta} - 8i\omega r - {}_{s}\lambda_{lm\omega} \right]_{-2} R_{lm\omega} = T_{lm\omega}, \tag{2.6}$$

$$\label{eq:linear_equation} \begin{split} &\left[\frac{1}{\sin\theta}\frac{d}{d\theta}\left(\sin\theta\frac{d}{d\theta}\right) - a^2\omega^2\sin^2\theta - \frac{(m-2\cos\theta)^2}{\sin^2\theta}\right. \\ &\left. + 4a\omega\cos\theta - 2 + 2ma\omega +_{-2}\lambda_{lm\omega}\right|_{-2}S_{lm\omega} = 0. \end{split}$$

Here  $K=(r^2+a^2)\omega-ma$ ,  $_{-2}\lambda_{lm\omega}$  is the spin-weighted spheroidal eigenvalue, and  $T_{lm\omega}$  is the decomposition of the (Newman-Penrose projection of the) stress-energy tensor. The spheroidal harmonic also has the normalization condition

$$\int_0^{\pi} |_{-2} S_{lm\omega}|^2 \sin\theta d\theta = 1. \tag{2.8}$$

Ultimately, these functions encode the first-order perturbation through composition of the quantity  $\psi_4$ , a certain Newman-Penrose projection of the Weyl tensor given by

$$\varrho^{-4}\psi_4 = \sum_{lm} \int e^{-i\omega t + im\varphi} S_{lm\omega}(\theta) R_{lm\omega}(r) d\omega, \quad (2.9)$$

where  $\varrho^{-1} = -(r - ia\cos\theta)$ . For more detail on the motivation and derivation behind these equations, see [38,39]. A deeper discussion is also given in [40].

Because the source motion is biperiodic, the Fourier integral collapses into a Fourier sum over the frequencies  $\omega = \omega_{mn} = m\Omega_{\varphi} + n\Omega_{r}$ . Then, the homogeneous form of the equation yields two independent solutions:  $_{-2}R_{lmn}^{-} = _{-2}R_{lmn}^{\rm in}$ , with causal (ingoing wave) behavior at the horizon, and  $_{-2}R_{lmn}^{+} = _{-2}R_{lmn}^{\rm up}$  with causal (outgoing wave) behavior at infinity. Both can be derived as infinite sums of hypergeometric functions using the MST formalism [14,39], which we briefly review below.

The spin-weighted spheroidal harmonics can be expanded in the spheroidicity  $a\omega$  (a 1.5PN quantity) by inserting a PN ansatz, applying standard boundary and normalization conditions, then solving a system of equations [51]. However, we expand them (along with their first and second  $\theta$  derivatives) simply by using the spheroidal harmonic package of the black hole perturbation toolkit [60]. The coefficient on each power of  $(a\omega)$  is given by a finite sum of spin-weighted spherical harmonics, which then takes an analytic value for specific choices of s, l, m, and  $\theta$ . See [40] for additional details.

# C. The MST homogeneous solutions and the source integration

The MST solution for  $_{-2}R^{+}_{lmn}$  can be expressed [39,51] as

$$\begin{split} {}_{-2}R^{+}_{lmn} &= e^{iz} \frac{z^{\nu+i(\epsilon+\tau)/2}}{(z-\epsilon\kappa)^{-2+i(\epsilon+\tau)/2}} \sum_{j=-\infty}^{\infty} a^{\nu}_{j} (2iz)^{j} \\ &\times \frac{\Gamma(j+\nu-1-i\epsilon)\Gamma(\nu+3+i\epsilon)}{\Gamma(j+\nu+3+i\epsilon)\Gamma(\nu-1-i\epsilon)} \\ &\times U(j+\nu-1-i\epsilon,2j+2\nu+2,-2iz), \quad (2.10) \end{split}$$

where U is the irregular confluent hypergeometric function,  $\epsilon = 2M\omega\eta^3$ ,  $z = (r-r_-)\omega\eta$ ,  $r_\pm = GM(1\pm\kappa)\eta^2$ ,  $\kappa = \sqrt{1-a^2}$ , and  $\eta = 1/c$ . The parameter  $\nu$  is the renormalized angular momentum, an eigenvalue chosen to make the series coefficients  $a_j$  (not to be confused with the spin parameter) converge as  $j \to \pm \infty$ . Both  $\nu$  and  $a_j$  are determined through continued fraction expansion [14,39], which leads to series

in  $\epsilon$  for both. The rest of the formula can then be expanded in both  $\epsilon$  and z, leading to a composite PN series in  $\eta$  (which by definition is a 0.5PN expansion parameter) [40,51].

Similarly, the solution for  $_{-2}R_{lmn}^{-}$  can be written as

$$\begin{split} {}_{-2}R^{-}_{lmn} &= e^{-iz+i\kappa\varepsilon} \bigg(\frac{\epsilon\kappa}{z}\bigg)^{i\tau+s} \bigg(1-\frac{\epsilon\kappa}{z}\bigg)^{-s-i(\epsilon+\tau)/2} \sum_{j=-\infty}^{\infty} a^{\nu}_{j2} F_{1} \\ &\times \bigg(j+\nu+1-i\tau,-j-\nu-i\tau,3-i\epsilon \\ &-i\tau,1-\frac{z}{\epsilon\kappa}\bigg). \end{split} \tag{2.11}$$

Here,  ${}_2F_1$  is the ordinary hypergeometric function, and the parameters  $\nu$  and  $a_i$  are the same as in Eq. (2.10).

The process of expanding these homogeneous solutions by collecting on powers of  $\eta$  is fully described in [40], based on the methods initially presented in [50,51,53], as well as [18]. From a computational perspective, the most important consideration is the fact that the homogeneous solutions as written in (2.10) and (2.11) contain many cumbersome z-independent factors that greatly complicate the expansion [18,40,51]. These factors will eventually cancel through division by the Wronskian and can thus be omitted from the start. One useful choice of normalization is given in [40], and the process is operationally similar to the Schwarzschild case, described in [18]. When computing the fluxes, the solutions must eventually be rescaled to produce the proper asymptotic behavior; however, in the metric reconstruction procedure this problem is avoided entirely, as all choices of normalization lead to the same result.

Once appropriately simplified, the homogeneous solutions can be used to complete the source integration [39,40]:

$$-2Z_{lmn}^{\pm} = \frac{1}{W_{lmn}T_r} \int_0^{T_r} \left[ (A_{nn0} + A_{\bar{m}n0} + A_{\bar{m}\bar{m}0}) R_{lmn}^{\mp} - (A_{\bar{m}n1} + A_{\bar{m}\bar{m}1}) \frac{dR_{lmn}^{\mp}}{dr} + A_{\bar{m}\bar{m}2} \frac{d^2 R_{lmn}^{\mp}}{dr^2} \right] \times e^{i\omega t - im\varphi(t)} dt.$$
(2.12)

The Wronskian  $W_{lmn}$  is given by

$$W_{lmn} = \frac{1}{\Delta} \left[ \frac{d_{-2}R_{lmn}^{+}}{dr} {}_{-2}R_{lmn}^{-} - \frac{d_{-2}R_{lmn}^{-}}{dr} {}_{-2}R_{lmn}^{+} \right], \qquad (2.13)$$

and source A functions (deriving from  $T_{lm\omega}$ ) are defined in Sasaki and Tagoshi [39] for generic orbits. The equatorial limits can be found in [40].

#### D. The Hertz potential in ingoing radiation gauge

The first-order generalized redshift invariant is a quantity that depends upon the behavior of the regularized metric perturbation along the particle's worldline. The global metric perturbation in radiation gauge can be derived using the CCK procedure [56–59]. In short, an intermediate Hertz potential  $\Psi$  is first constructed from products of the normalization coefficients  $_{-2}Z^{\pm}_{lmn}$ , the homogeneous solutions  $_{-2}R^{\pm}_{lmn}$ , and spin-weighted spheroidal harmonics  $_{-2}S_{lmn}$ . The Hertz potential is then transformed through a sequence of linear operations to yield the metric perturbation.

The s=-2 solutions are most easily adapted to the use of ingoing radiation gauge, whose Hertz potential in vacuum is a solution of the homogeneous s=-2 Teukolsky equation [68,69]. Thus, it can be written in the generic form

$$\Psi^{\pm} = \frac{1}{\sqrt{2\pi}} \sum_{lmn} \Psi^{\pm}_{lmn-2} R^{\pm}_{lmn}(r)_{-2} S^{\pm}_{lmn} e^{im\varphi - i\omega t}, \quad (2.14)$$

for some undetermined coefficients  $\Psi_{lmn}^{\pm}$ . In general, it is also governed by the following fourth-order inhomogeneous partial differential equations [68,69]:

$$\frac{1}{2}(\mathbf{D})^4 \bar{\Psi} = \psi_0,$$

$$\frac{1}{8} [\tilde{\mathcal{L}}^4 \bar{\Psi} - 12M \partial_t \Psi] = \varrho^{-4} \psi_4, \qquad (2.15)$$

where

$$\mathbf{D} = \frac{r^2 + a^2}{\Delta} \partial_t + \partial_r + \frac{a}{\Delta} \partial_\varphi = l^\mu \partial_\mu, \qquad (2.16)$$

$$\tilde{\mathcal{L}}^4 = \tilde{\mathcal{L}}_1 \tilde{\mathcal{L}}_0 \tilde{\mathcal{L}}_{-1} \tilde{\mathcal{L}}_{-2} \tag{2.17}$$

$$\tilde{\mathcal{L}}_{q} = -\partial_{\theta} - q \cot \theta + i \csc \theta \partial_{\varphi} + i a \sin \theta \partial_{t}, \qquad (2.18)$$

and the overbar denotes complex conjugation.

The angular equation can be used to identify the coefficients  $\Psi^{\pm}_{lmn}$ . First, we must note that the complex conjugate can be expressed as

$$\begin{split} \bar{\Psi}^{\pm} &= \frac{1}{\sqrt{2\pi}} \sum_{lmn} \bar{\Psi}^{\pm}_{lmn-2} \bar{R}^{\pm}_{lmn}(r)_{-2} \bar{S}^{\pm}_{lmn} e^{-im\varphi + i\omega t} \\ &= \frac{1}{\sqrt{2\pi}} \sum_{lmn} \bar{\Psi}^{\pm}_{lmn-2} R^{\pm}_{l-m-n}(r) (-1)^{m}_{2} S^{\pm}_{l-m-n} e^{-im\varphi + i\omega t} \\ &= \frac{1}{\sqrt{2\pi}} \sum_{lmn} \bar{\Psi}^{\pm}_{l-m-n-2} R^{\pm}_{lmn}(r) (-1)^{m}_{2} S^{\pm}_{lmn} e^{im\varphi - i\omega t}, \end{split}$$

$$(2.19)$$

where we used the identity  ${}_s\bar{S}_{lmn}=(-1)^{m+s}{}_{-s}S_{l-m-n}$  and took  $(m,n)\to (-m,-n)$  in the sum. Then, the  $\tilde{\mathcal{L}}^4$  operator is simplified using the Teukolsky-Starobinsky identity from Chandrasekhar [70], or

$$\tilde{\mathcal{L}}^{4}{}_{2}S_{lmn} = F(_{-2}S_{lmn}) \tag{2.20}$$

for

$$F^{2} = ({}_{-2}\lambda_{lmn})^{2}({}_{-2}\lambda_{lmn} + 2)^{2} + 8a\omega(m - a\omega)({}_{-2}\lambda_{lmn}) \times [5_{-2}\lambda_{lmn} + 6] + 48a^{2}\omega^{2}[2({}_{-2}\lambda_{lmn}) + 3(m - a\omega)^{2}].$$
(2.21)

With these steps the amplitudes are found to satisfy the relation

$$\frac{1}{8}[F(-1)^m\bar{\Psi}_{l-m-n} + 12M(i\omega)\Psi_{lmn}] = {}_{-2}Z_{lmn}^{\pm}. \quad (2.22)$$

This can be inverted to isolate  $\Psi_{lmn}$  by taking a linear combination of  $Z_{lmn}$  and  $Z_{l-m-n}$ . We get

$$\Psi_{lmn} = 8 \frac{(-1)^m F Z_{l-m-n} - 12 M i \omega Z_{lmn}}{F^2 + 144 M^2 \omega^2}$$

$$= 8 \left[ \frac{(-1)^{l+m} F - 12 M i \omega}{F^2 + 144 M^2 \omega^2} \right] Z_{lmn}, \qquad (2.23)$$

where the last step applied the identity  $Z_{l-m-n} = (-1)^l Z_{lmn}$ . Thus, the coefficients are relatively easy to retrieve from the s=-2 homogeneous solutions and normalization constants.

## E. The metric perturbation in ingoing radiation gauge

With the Hertz potential computed, the metric perturbations in ingoing radiation gauge follow as [71]

$$p_{\mu\nu} = -\left\{ \ell_{\mu}\ell_{\nu}(\boldsymbol{\delta} + \bar{\alpha} + 3\beta - \tau)(\boldsymbol{\delta} + 4\beta + 3\tau) + m_{\mu}m_{\nu}(\boldsymbol{D} - \varrho)(\boldsymbol{D} + 3\varrho) - \ell_{(\mu}m_{\nu)}[(\boldsymbol{\delta} - 2\bar{\alpha} + 2\beta - \tau)(\boldsymbol{D} + 3\varrho) + (\boldsymbol{D} + \bar{\varrho} - \varrho) \right\} \times (\boldsymbol{\delta} + 4\beta + 3\tau)$$

$$\times (\boldsymbol{\delta} + 4\beta + 3\tau)$$

$$(2.24)$$

The various operators, tetrad components, and spin coefficients are defined in the Newman-Penrose formalism [72]. Explicitly, we have

$$\ell^{\alpha} = \frac{1}{\Delta} (r^{2} + a^{2}, \Delta, 0, a),$$

$$m^{\alpha} = -\frac{\bar{\varrho}}{\sqrt{2}} \left( ia \sin \theta, 0, 1, \frac{i}{\sin \theta} \right),$$

$$\delta = m^{\mu} \partial_{\mu} = \frac{ia \sin \theta}{\sqrt{2} (r + ia \cos \theta)} \partial_{t} + \frac{1}{\sqrt{2} (r + ia \cos \theta)} \partial_{\theta} + \frac{i}{\sqrt{2} (r + ia \cos \theta) \sin \theta} \partial_{\varphi},$$

$$\varrho = \frac{-1}{r - ia \cos \theta}, \qquad \tau = \frac{-ia \sin \theta}{\sqrt{2} \Sigma}, \qquad \beta = \frac{\cot \theta}{2\sqrt{2} (r + ia \cos \theta)},$$

$$\alpha = \frac{ia \sin \theta}{\sqrt{2} (r - ia \cos \theta)^{2}} - \frac{\cot \theta}{2\sqrt{2} (r + ia \cos \theta)}.$$
(2.25)

Note that the metric perturbation in ingoing radiation gauge satisfies the conditions  $\ell^{\mu}p_{\mu\nu}=0$  and  $g^{\mu\nu}_{\text{Kerr}}p_{\mu\nu}=0$ , where  $g^{\mu\nu}_{\text{Kerr}}$  is the (inverse) background metric.

Once these tetrad terms, along with the modal form of the Hertz potential, are inserted into (2.24), the result is an unwieldy combination of  $_{-2}R_{lmn}$ ,  $\partial_{r-2}R_{lmn}$ ,  $\partial_{r-2}^2R_{lmn}$  and  $_{-2}S_{lmn}$ ,  $\partial_{\theta-2}S_{lmn}$ ,  $\partial_{\theta-2}^2S_{lmn}$  multiplying factors involving r,  $\omega$ , m, and  $\theta$ . The full expression simplifies in the equatorial plane, but the result remains too large to display here. Nevertheless, once the metric perturbation is derived in analytic form, the process of completing its PN expansion is straightforward, if cumbersome.

### III. GENERAL-I EXPANSIONS

The MST formalism described in the previous section provides mode functions for specific l. In the dissipative

sector [18,40], PN expansions of the relevant observables (e.g., the fluxes) possess leading behavior that increases with l. Thus, an expansion to any particular desired PN order requires calculation of only finite values of l. Unfortunately, this phenomenon does not recur in the conservative dynamics, as the leading PN order of the local metric perturbations  $p_{\mu\nu}^l(\chi)$  is constant in l. As a result, we must compute expansions for all values of l to determine the full metric perturbation  $p_{\mu\nu}(\chi)$ , which is prohibitively difficult using the MST approach. In the Schwarzschild case, it proved possible to use a PN ansatz solution in the RWZ equation to obtain expansions that remained general in l, which could then be iterated through the rest of the process and summed over all values of l when necessary [20,44-46]. It turns out that a similar approach can be completed in the Kerr problem [51], though with several added difficulties over the Schwarzschild background. We detail the full procedure below.

## A. The homogeneous solutions and normalization constants

As in the Schwarzschild case [44,46], we start by introducing a PN ansatz for the homogeneous solutions of the Teukolsky equation. Following [51], we choose

$${}_{s}R_{lmn}^{-} = \left(\frac{\bar{\epsilon}}{\bar{z}}\eta^{2}\right)^{-\nu+s} (1 + A_{1}\eta + A_{2}\eta^{2} + \dots + A_{2l}\eta^{2l} + \mathcal{O}(\eta^{2l+1})),$$

$${}_{s}R_{lmn}^{+} = (\bar{z}\eta)^{-\nu-1-s} (1 + B_{1}\eta + B_{2}\eta^{2} + \dots + B_{2l}\eta^{2l} + \mathcal{O}(\eta^{2l+1})), \tag{3.1}$$

where the  $A_i$  and  $B_i$  are functions of  $(\bar{z}, \bar{\epsilon}, l, m, a), \bar{z} = r\omega$ , and  $\bar{\epsilon} = 2GM\omega$ . Once  $\nu$  is found using the continued

fraction method for general l, these expressions are plugged into the (s = -2) homogeneous Teukolsky equation,

$$\Delta^{3} \frac{d}{dr} \left( \frac{1}{\Delta} \frac{dR_{lmn}}{dr} \right) + [K^{2} + 4i(r - M)K - (8i\omega r + {}_{-2}\lambda_{lmn})\Delta]R_{lmn} = 0,$$
(3.2)

and solved order by order. Note that we multiplied the original Teukolsky equation by  $\Delta$  to simplify appearances of  $\eta$ . Unfortunately, the ansatz does not fully apply the boundary conditions, which is why it breaks down after some l-dependent PN order [44–46,51]. If a target PN order P is set, the ansatz will be useless for  $l \lesssim P$ . Thus, those values of l must be determined separately with the MST formalism.

Proceeding in this way, we obtain a general-l PN expansion for  $\nu$ , which begins

$$\nu = l + \frac{24 + 13l + 28l^2 + 30l^3 + 15l^4}{6l + 10l^2 - 20l^3 - 40l^4 - 16l^5} \epsilon^2 + \frac{(108 + 18l + 17l^2 + 3l^3 + 14l^4 + 15l^5 + 5l^6)}{l^2(1 + l)^2(6 + l - 29l^2 - 6l^3 + 20l^4 + 8l^5)} ma \ \epsilon^3 + \mathcal{O}(\epsilon^4)$$
(3.3)

and obtain the general-l expansions for the mode functions, which likewise begin

$$\begin{split} &_{-2}R_{lmn}^{+,\text{ser}} = (\bar{z}\eta)^{l-1}{}_{-2}R_{lmn}^{+} = 1 - \frac{2i\bar{z}}{l}\eta + \frac{\bar{\epsilon}l(2l-1)(l^2-1+2iam) + (l^2-7l-8)\bar{z}^3}{2l(1+l)(2l-1)\bar{z}}\eta^2 - \frac{i(l-3)\bar{z}^3}{(l-1)l(2l-1)}\eta^3 \\ &\quad + \frac{1}{8\bar{z}^2} \left[ \frac{\bar{\epsilon}^2(2l^4 - (a^2-4)l^3 - 9a^2m^2 + l^2(8iam-2) + l(12iam-4-a^2(m^2-1)))}{(1+l)(3+2l)} + \frac{(32-17l+l^2)\bar{z}^6}{l(2l-3)(1-3l+2l^2)} \right. \\ &\quad + \frac{2\bar{\epsilon}(14l^4+l^5+16iam+16l(1-iam)+l^3(-7+2iam)+l^2(-4+12iam))\bar{z}^3}{l^3(-1+l+2l^2)} \eta^4 + \mathcal{O}(\eta^5), \\ &\quad - 2R_{lmn}^{-,\text{ser}} = \left( \frac{\bar{\epsilon}}{\bar{z}}\eta^2 \right)^{l+2} {}_{-2}R_{lmn}^{-} = 1 + \frac{2i\bar{z}}{1+l}\eta - \frac{1}{2\bar{z}} \left[ \bar{\epsilon}\left(2+l+\frac{2iam}{l}\right) + \frac{(9+l)\bar{z}^3}{3+5l+2l^2} \right] \eta^2 - \frac{i(4+l)\bar{z}^3}{(2+l)(3+5l+2l^2)} \eta^3 \\ &\quad + \left[ \frac{\bar{\epsilon}^2(l(1+l)(2+l)(a^2+2l-2) + 4ia(1+l)(2l-1)m + a^2(l-8)m^2)}{l(2l-1)} + \frac{(50+l(19+l))\bar{z}^6}{(1+l)(2+l)(3+2l)(5+2l)} \right. \\ &\quad + \frac{2\bar{\epsilon}(l(1+l)(-48+l(-43+(-10+l)l)) + 2ia(-21+l(-17+(-3+l)l))m)\bar{z}^3}{l(1+l)^3(3+2l)} \eta^4 + \mathcal{O}(\eta^5). \end{aligned}$$

Here, we defined  $R_{lmn}^{\rm ser}$  as the normalized PN series that begin at  $\mathcal{O}(1)$ , which are more convenient to manipulate at each step of the calculation than the original series with l-dependent PN orders. Eventually, all l-dependent powers of  $\eta$  will cancel in the metric perturbation due to their corresponding presence in the Wronskian.

Once expanded, the general-l homogeneous solutions can be evaluated along the geodesic orbit to compute the Wronskian and prepare for the source integration (at which point the series will be defined in terms of v and e, as in the specific-l case). However, the source terms themselves carry one additional complication: expansions of the

spin-weighted spheroidal harmonics become large and unwieldy for general l and m, which significantly slows the procedure. We avoid this problem by leaving  $_{-2}S_{lmn}$  and its derivatives as unevaluated parameters until the final step of metric reconstruction. Once the metric perturbation is expanded, we handle products of the spheroidal harmonics together in the sum over m.

### B. Sums of spin-weighted spheroidal harmonics over *m*

The general-l expansions are carried through the source integration and then used to construct the metric perturbation (2.24) just as in the specific-l case. Computationally,

the source integration is completed in one step, and then the expansions for  $Z_{lmn}^+, R_{lmn}^+, S_{lmn}$ , and the Fourier kernel  $e^{im\varphi-i\omega t}$  are directly included in the formula for the metric perturbation. Each n is calculated individually, as only finite n modes are required to reach any particular order in e, and then the set is summed at the end. We also split up the calculation over the nine spheroidal harmonic products  $[S_{lmn}, \partial_{\theta}S_{lmn}, \partial_{\theta\theta}S_{lmn}]$  within the normalization constant  $Z_{lmn}^+$ , multiplied against the same three terms within the rest of the metric perturbation (2.24)] that are left unevaluated until the end. Even with this extensive segregation of terms, the PN expansion for each individual component serves as the computational bottleneck for this procedure. In particular, the  $(n = 1, S_{lmn} \times S_{lmn})$  part of each metric perturbation requires about eight days and 10 GB of memory to reach either  $6PN/e^{16}$  or  $8PN/e^{10}$  on the University of North Carolina (UNC) supercomputing cluster Longleaf. (Fortunately, it is trivial to parallelize over the various combinations of n and  $S_{lmn}$ .)

Once all the components are calculated, we are left with the task of summing the mode expressions over m to obtain  $p_{\mu\nu}^l$ . This process is nontrivial, as each m mode contains products of spin-weighted spheroidal harmonics (still unexpanded), and the sum must be taken from -l to l for general l. In the Schwarzschild-RWZ problem, we faced a similar obstacle, having to complete sums of the form

$$\sum_{m=-l}^{l} m^{N} Y_{lm}(\pi/2, 0)^{2}, \qquad \sum_{m=-l}^{l} m^{N} \partial_{\theta} Y_{lm}(\pi/2, 0)^{2}, \quad (3.5)$$

where  $Y_{lm}$  is the standard scalar spherical harmonic,

$$Y_{lm}(\theta, \varphi) = \sqrt{\frac{(2l+1)(l-m)!}{4\pi(l+m)!}} P_l^m(\cos\theta) e^{im\varphi},$$
 (3.6)

and N is any positive integer. In that case the first sum can be derived using a special case of the spherical harmonic addition theorem [20]:

$$\sum_{m=-l}^{l} e^{im\varphi} Y_{lm}(\pi/2,0)^2 = \left(\frac{2l+1}{4\pi}\right) P_l(\cos\varphi), \quad (3.7)$$

with the result for each value of N corresponding to a term in the Taylor expansion of this formula about  $\varphi = 0$ . The second summation could then be derived from derivatives of the spherical harmonic addition theorem, or from a hypergeometric generating function [73].

In the Kerr-Teukolsky formalism, we now encounter sums like

$$T_{00}^{0} = \sum_{m=-l}^{l} m^{N}_{-2} S_{lm}(\pi/2)^{2}, \qquad T_{00}^{1} = \sum_{m=-l}^{l} (-1)^{l+m} m^{N}_{-2} S_{lm}(\pi/2)^{2},$$

$$T_{01}^{0} = \sum_{m=-l}^{l} m^{N}_{-2} S_{lm}(\pi/2) (\partial_{\theta-2} S_{lm}(\pi/2)), \qquad T_{01}^{1} = \sum_{m=-l}^{l} (-1)^{l+m} m^{N}_{-2} S_{lm}(\pi/2) (\partial_{\theta-2} S_{lm}(\pi/2)),$$

$$T_{11}^{0} = \sum_{m=-l}^{l} m^{N} (\partial_{\theta-2} S_{lm}(\pi/2))^{2}, \qquad T_{11}^{1} = \sum_{m=-l}^{l} (-1)^{l+m} m^{N} (\partial_{\theta-2} S_{lm}(\pi/2))^{2}, \qquad (3.8)$$

and so on for sums  $T_{02}^{0/1}$ ,  $T_{12}^{0/1}$ ,  $T_{22}^{0/1}$ . Note that we have suppressed the n index for convenience and that the factors of  $(-1)^{l+m}$  can be traced back to the Hertz potential coefficients in (2.23). Unfortunately, the spin-weighted spheroidal harmonics do not have a known addition theorem, and it is unlikely that any comparable formula like it can be derived. In fact,  $_{-2}S_{lm}(\pi/2)$  does not even have a known analytic form for specific values of l and m.

Nevertheless, progress can be made by PN expanding  $S_{lm}$  and its derivatives, now for general-lm, yielding series like [51,60]

$$\begin{split} {}_sS_{lm}(\theta) &= {}_sY_{lm}(\theta) + \frac{s}{\sqrt{1+2l}} \bigg( \frac{\sqrt{l^2-m^2}\sqrt{l^2-s^2}}{l^2\sqrt{2l-1}} {}_sY_{(l-1)m}(\theta) - \frac{\sqrt{(l+1)^2-m^2}\sqrt{(l+1)^2-s^2}}{(1+l)^2\sqrt{3+2l}} {}_sY_{(l+1)m}(\theta) \bigg) a\omega \\ &+ \frac{1}{2} \left[ -\frac{\sqrt{l^2-m^2}\sqrt{1-2l+l^2-m^2}(l-2s^2)\sqrt{l^2-s^2}\sqrt{1-2l+l^2-s^2}}{(1-2l)^2(-1+l)l^2\sqrt{-3+2l}\sqrt{1+2l}} {}_sY_{(l-2)m}(\theta) + {}_sY_{(l-1)m}(\theta) \right. \\ &\times \frac{2ms\sqrt{(l^2-m^2)(l^2-s^2)}(l^2-2s^2)}}{l^4\sqrt{4l^2-1}(l^2-1)} + s^2 \bigg( \frac{(l^2-m^2)(l^2-s^2)}{l^4(1-4l^2)} - \frac{[(l+1)^2-m^2][(l+1)^2-s^2]}{(1+l)^4(3+8l+4l^2)} \bigg) {}_sY_{lm}(\theta) \end{split}$$

$$-\frac{2m\sqrt{1+2l+l^2-m^2}s(1+2l+l^2-2s^2)\sqrt{1+2l+l^2-s^2}}{l(1+l)^4(2+l)\sqrt{1+2l}\sqrt{3+2l}}sY_{(l+1)m}(\theta) + \frac{\sqrt{[(l+1)^2-m^2][(l+2)^2-m^2]}\sqrt{[(l+1)^2-s^2][(l+2)^2-s^2]}(1+l+2s^2)}{(1+l)^2(2+l)\sqrt{1+2l}(3+2l)^2\sqrt{5+2l}}sY_{(l+2)m}(\theta)\Big](a\omega)^2 + \cdots.$$
(3.9)

Derivatives of  ${}_sS_{lm}(\theta)$  are applied directly to the terms in the series. Thus, when products of these series are taken, we will be left with sums over spin-weighted spherical harmonics, instead of spheroidal harmonics.

Spin-weighted spherical harmonics are also unlikely to yield straightforward summation formulas, and the reference [51] handled these sums using *Mathematica*'s FINDSEQUENCEFUNCTION. However, it turns out that exact, if cumbersome, formulas can be derived analytically by using the spin-weighted spherical harmonic definition to transform back to scalar spherical harmonics. Explicitly,

$$_{s-1}Y_{lm} = \frac{(\sin\theta)^{-s}}{\sqrt{(l+s)(l-s+1)}} \left[ \frac{\partial}{\partial\theta} - \frac{i}{\sin\theta} \frac{\partial}{\partial\varphi} \right] ((\sin\theta)^{s} {}_{s}Y_{lm}). \tag{3.10}$$

Thus, s = -2 can be expressed in terms of s = 0 as

$${}_{-2}Y_{lm} = \sqrt{\frac{(l-2)!}{(l+2)!}} \left[ \partial_{\theta}^{2} Y_{lm} + \frac{2m - \cos \theta}{\sin \theta} \partial_{\theta} Y_{lm} + \frac{m^{2} - 2m \cos \theta}{(\sin \theta)^{2}} Y_{lm} \right].$$
(3.11)

Substitution of this relation and (3.9) into the summation formulas (3.8) would then yield products of scalar spherical harmonics alone, which are closely connected to the spherical harmonic addition theorem. However, the expression (3.9) contains multiple values of the first harmonic number ( $l, l \pm 1, l \pm 2$ , etc.), while the addition theorem (3.7) only explicitly covers products of terms with identical harmonic numbers. This last problem can be resolved by using the well-known scalar spherical harmonic identity,

$$Y_{(l+1)m} = \cos \theta \sqrt{\frac{(2l+1)(2l+3)}{(l+1)^2 - m^2}} Y_{lm} - \sqrt{\frac{(2l+3)(l^2 - m^2)}{(2l-1)[(l+1)^2 - m^2]}} Y_{(l-1)m}.$$
(3.12)

We also find it convenient to eliminate all derivative terms using identities of the following form:

$$\begin{split} \sin\theta \frac{d}{d\theta} Y_{lm} &= l \cos\theta Y_{lm} - \sqrt{\frac{(2l+1)(l^2 - m^2)}{(2l-1)}} Y_{(l-1)m}, \\ \sin\theta \frac{d}{d\theta} Y_{lm} &= -(l+1) \cos\theta Y_{lm} \\ &+ \sqrt{\frac{(2l+1)[(l+1)^2 - m^2]}{(2l+3)}} Y_{(l+1)m}. \end{split} \tag{3.13}$$

In total we make a sequence of identity transformations until all terms are of the form  $Y_{lm}$  and  $Y_{(l-1)m}$ . Then, the remaining products will involve only  $m^N Y_{lm}^2$  and  $m^N Y_{(l-1)m}^2$ , which are trivial to execute using the addition theorem. In particular, we find that no square root terms appear in the final product and that the cross terms vanish, as  $Y_{lm}(\pi/2)$  is 0 whenever (l+m) is odd, meaning one of  $Y_{lm}(\pi/2)$  and  $Y_{(l-1)m}(\pi/2)$  is always 0. Parity considerations also clarify how to account for factors of  $(-1)^m$ —these terms simplify to become overall factors of  $(-1)^l$  or  $(-1)^{l-1}$ , as appropriate. Then, the full term  $(-1)^{l+m}$  simply contributes  $(-1)^{2l} = 1$  or  $(-1)^{2l-1} = -1$  to each component of the sum.

Thus, to summarize, we expand the spin-weighted spheroidal harmonics into series of spin-weighted spherical harmonics; then, we use the definition of each  $_{-2}Y_{lm}$  to reexpress it in terms of  $Y_{lm}$ . Next,  $\theta$  derivatives and distant values of the first harmonic number are eliminated using identities, at which point the standard spherical harmonic addition theorem can be used to complete the summation. Once the metric perturbation is summed over m, the general-l expansion for  $p_{\mu\nu}^l$  will be ready for use in the construction of the redshift.

# IV. METRIC COMPLETION AND REGULARIZATION

With the procedure established for the specific-*l* (MST) and the general-*l* (ansatz) parts of the metric perturbation, we are left with two remaining considerations: the completion of the metric (monopole and dipole terms) and regularization procedure. We briefly cover those issues here.

#### A. Nonradiative modes

The Teukolsky formalism is only valid for the modes  $l \ge s$ . Notably, it omits the corrections to the mass monopole and dipole of the primary (informally referred to as the l = 0 and l = 1 modes), which must be derived separately. The full completion part  $p_{\mu\nu}^{\text{comp}}$  was first derived in [71]. It is given by

$$p_{tt}^{\text{comp+}} = \frac{2r}{\Sigma^{2}} [(r^{2} + 3a^{2} \cos^{2} \theta)\delta M - 2a \cos^{2} \theta \delta J],$$

$$p_{rr}^{\text{comp+}} = \frac{2r}{M\Delta^{2}} \{ [M(r^{2} + 3a^{2} \cos^{2} \theta) + a^{2}r \sin^{2} \theta]\delta M - a[r \sin^{2} \theta + 2M \cos^{2} \theta]\delta J \},$$

$$p_{\theta\theta}^{\text{comp+}} = -\frac{2a}{M} \cos^{2} \theta (a\delta M - \delta J),$$

$$p_{\phi\phi}^{\text{comp+}} = -\frac{2a}{M\Sigma^{2}} \sin^{2} \theta \{ a[\Sigma^{2} + Mr \sin^{2} \theta (r^{2} - a^{2} \cos^{2} \theta)]\delta M - (\Sigma^{2} + 2Mr^{3} \sin^{2} \theta)\delta J \},$$

$$p_{t\phi}^{\text{comp+}} = -\frac{2r}{\Sigma^{2}} \sin^{2} \theta [2a^{3} \cos^{2} \theta \delta M + (r^{2} - a^{2} \cos^{2} \theta)\delta J],$$
(4.1)

where  $p_{\mu\nu}^{\rm comp}=p_{\mu\nu}^{\rm comp+}\Theta[r-r_p(t)]$ . After a lengthy calculation, [71] confirmed the expected result that  $\delta M=\mu\mathcal{E}$  and  $\delta J=\mu\mathcal{L}$ .

Because we are only interested in the local perturbation, we can restrict these expressions to the equatorial plane, which simplifies the result to

$$\begin{split} p_{tt}^{\text{comp+}} &= \frac{2\delta M}{r}, \\ p_{rr}^{\text{comp+}} &= \frac{2r^2}{M\Delta^2}[(Mr+a^2)\delta M - a\delta J], \\ p_{\theta\theta}^{\text{comp+}} &= 0, \\ p_{\phi\phi}^{\text{comp+}} &= -\frac{2a}{Mr}[a(r+M)\delta M - (r+2M)\delta J], \\ p_{t\phi}^{\text{comp+}} &= -\frac{2}{r}\delta J. \end{split} \tag{4.2}$$

Actually, there is another nonradiative contribution termed  $p_{\mu\nu}^{\rm gauge}$  that was discussed at length in [74]. However, this term is 0 for all  $r>r_p$  and therefore does not affect the value of the redshift, which is calculated here in the limit  $r\to r_p$  from above. The authors of [74] also note that the redshift combination  $p_{\mu\nu}^R u^\mu u^\nu$  must be continuous across  $r=r_p$ , so that the gauge portion is not needed. On the other hand, the spin-precession invariant [75,76] is typically regularized through an upper-lower-limit averaging procedure, so it is likely that  $p_{\mu\nu}^{\rm gauge+}$  will have to be included in that calculation.

### B. Mode-sum regularization

Thus far, the expressions given for the metric perturbation in ingoing radiation gauge have referred to the full retarded field. This field formally diverges at the location of the particle, a property that becomes apparent when the l modes are summed from l=0 to  $l=\infty$ . Local gauge

invariant quantities derived from these modes then exhibit the same behavior. Instead, from the full retarded field we must extract the so-called regular field, which defines the effective metric experienced by the smaller body.

The regular part of the metric is derived through regularization, which can be achieved in a number of ways. One popular approach was given by Detweiler and Whiting [77], which chooses a particular split of regular and singular fields,

$$p_{uv}(x) = p_{uv}^S(x) + p_{uv}^R(x). \tag{4.3}$$

With this choice the singular field  $p_{\mu\nu}^S(x)$  satisfies the same inhomogeneous field equation as  $p_{\mu\nu}(x)$  but with different boundary conditions, while  $p_{\mu\nu}^R$  then solves the homogeneous field equations. The orbiting particle then travels on the Kerr metric plus the perturbation  $p_{\mu\nu}^R$ .

Determination of the singular field is a difficult process [78]. In first-order BHPT a common approach is the mode-sum regularization procedure [79,80], which exploits the fact that the individual l modes of the retarded metric perturbation are finite. The part of the l dependence that diverges in the infinite sum is subtracted off each l mode, so that the full sum remains finite.

The l dependence of the singular field can be expressed as an expansion about  $l=\infty$ . The metric perturbation itself will have a leading coefficient independent of l, which will obviously diverge in the sum over l. Each derivative of the singular field with respect to any of the coordinates will increase the divergence by a power of l. In Lorenz gauge, it is known that the large-l expansion can be manipulated into a form such that only the divergent terms are needed to obtain the regular field—the rest will vanish in a sum over all l. Interestingly, in a numerical calculation of finite l, the higher-order terms (regularization parameters) can improve convergence [78]. However, our analytic calculation will

complete the infinite sum over all l, so only the divergent terms are needed.

The redshift invariant is directly proportional to the metric perturbation, so what remains is to determine the l-independent coefficient (the leading regularization parameter) in its expansion about  $l = \infty$ . In fact, this can be done using our general-l PN series. This series is expanded in l, and the leading coefficient produces the singular field. There is a subtlety involving our use of radiation gauge, instead of the more established Lorenz gauge, as the former is related to the latter by an irregular gauge transformation [81]. However, it was noted by Detweiler [42] that the regularization scheme becomes gauge invariant when working with certain gauge invariant quantities, the redshift among them. This l-expansion approach to regularization has already been used successfully to construct the PN series for redshift invariant of eccentric, equatorial (Kerr) EMRIs in [53,54].

### V. THE GENERALIZED REDSHIFT INVARIANT

#### A. Background and implementation

The generalized redshift invariant has the same definition and interpretation for eccentric, equatorial inspirals on a Kerr background as it does for eccentric inspirals on a Schwarzschild background. Thus, the corresponding discussion in our previous Schwarzschild work [20], based on prior derivations in [27,47,48], is sufficient to understand the meaning and significance of the PN expansion presented here. Nevertheless, we will recapitulate the development of the generalized redshift invariant here for the sake of completeness.

The redshift invariant  $u^t$  was originally constructed for quasicircular inspirals [42,82]. Note that this quantity is precisely the inverse of the redshift itself,  $z=1/u^t$ . For eccentric orbits, Barack and Sago discovered that the proper-time average over a radial libration  $\langle u^t \rangle_{\tau}$  provided the more appropriate gauge invariant measure of the conservative dynamics. This average is equal to the coordinate-time period,  $T_r$ , divided by the proper-time period,  $T_r$ . To subleading order in the mass ratio, this quotient is given by [47,48]

$$\langle u^t \rangle_{\tau} = \frac{T_r}{T_r + \Delta T_r} = \frac{T_r}{T_r} - \Delta T_r \frac{T_r}{T_r^2} = \langle u^t \rangle_{\tau}^0 + \langle u^t \rangle_{\tau}^1. \quad (5.1)$$

Note that the coordinate-time period  $T_r$  is not corrected because the frequencies are held fixed from zeroth to first order (which is necessary for the gauge invariance of the redshift invariant [47]). The leading term  $\langle u^t \rangle_{\tau}^0$  is merely the value of the redshift invariant for geodesic orbits, which is trivial to calculate using the Darwin parametrization described in Sec. II A. The second term, which incorporates the effects of the first-order conservative self-force, can be shown to take the form [47,48]

$$\Delta \mathcal{T}_r = -\mathcal{T}_r \left\langle \frac{1}{2} p_{\mu\nu}^R u^\mu u^\nu \right\rangle_{\tau}. \tag{5.2}$$

This formula is the same for eccentric, equatorial orbits on both Schwarzschild and Kerr backgrounds. Thus, the correction to the generalized redshift invariant follows directly from the regularized metric perturbation, which we have detailed extensively in previous sections for the purpose of PN expansion.

As mentioned before, this particular gauge-invariant quantity encodes important details of the conservative motion of the system. The first-order conservative dynamics contribute at  $\mathcal{O}(\varepsilon^0)$  in the cumulative EMRI phase, a level needed for the creation of accurate waveform templates in the LISA mission, making the redshift invariant especially valuable [1]. In addition, there is an exact correspondence between the PN expansion of  $\langle u^t \rangle_{\tau}^1$  and several important quantities in EOB theory. For instance, the eccentric part of  $\langle u^t \rangle_{\tau}^1$  can be used to derive the expansion of the  $Q(1/r, p_r; \nu)$  EOB potential, which governs the deviation from geodesic behavior in the EOB Hamiltonian [26,27,53,62,83]. The transformation between these quantities is outlined in [26]. The circular spin-dependent part, meanwhile, is critical to the radial equatorial potential  $A(r, m_1, m_2, S_1, S_2)$  and the main spinorbit coupling potential  $G_S(r, m_1, m_2, S_1, S_2)$  [53]. The eccentric spin-dependent part is expected to be more fruitful still, though the precise transcription scheme has not yet been elucidated [54].

The last remaining task is to implement the mode-sum regularization scheme in order to ensure a proper, convergent sum over the l modes of  $\langle u^t \rangle_{\tau}^1$ . We choose to regularize the final averaged product, which is already in gauge invariant form:

$$\left\langle \frac{1}{2} p_{\mu\nu}^R u^\mu u^\nu \right\rangle_{\tau} = \sum_{l=0}^{\infty} \left\langle \frac{1}{2} \left( p_{\mu\nu}^l - p_{\mu\nu}^{S,l} \right) u^\mu u^\nu \right\rangle_{\tau}$$
$$= \sum_{l=0}^{\infty} \left\langle \frac{1}{2} p_{\mu\nu}^l u^\mu u^\nu \right\rangle_{\tau} - \left\langle H_{[0]} \right\rangle_{\tau}. \tag{5.3}$$

The singular field contribution is thus distilled down to an l-independent constant, equal to its leading behavior in a large-l expansion, in accordance with the observations of the previous section.

Analytic derivations of the singular part of the redshift invariant have been made [27,47,78], but these have generally utilized a decomposition over spherical harmonics, while our l modes derive from spin-weighted spheroidal harmonics. For circular, equatorial orbits on a Kerr background, Kavanagh, Ottewill, Wardell derived the spin-weighted spheroidal form of  $H_{[0]}$  to 13PN order [51]. We chose to use the general-l ansatz expansion to extract the large-l behavior directly, as has been done in [53,54]. Our expanded  $H_{[0]}$  is confirmed to match the analytic result

of [51] in the circular orbit limit. The PN series for the orbital average of  $H_{[0]}$  begins

$$\begin{split} \left\langle H_{[0]} \right\rangle_{\tau} &= (1-e^2)v^2 - \left[ (1-e^2)^2 - \frac{3}{4}(1-e^2)^{3/2} \right] v^4 \\ &- 2\tilde{a}[(1-e^2)^2 - (1-e^2)^{3/2}] v^5 \\ &+ \left[ (1-e^2)^{3/2} \left( \frac{153}{64} + \frac{3}{4}\tilde{a}^2 + \frac{267e^2}{128} \right) \right. \\ &- (1-e^2)(3+\tilde{a}^2+e^2) \left] v^6 + \mathcal{O}(v^7). \end{split} \tag{5.4}$$

This constant is then subtracted off at each value of l from l=0 to  $l=\infty$ . Note that this covers all three regimes of calculation: the metric completion piece (l=0 and l=1), the MST specific-l solutions from l=2 to l=7, and the general-l ansatz solution from l=8 to  $l=\infty$ . The form of the summands will involve products and quotients of polynomials in l, which are trivial to sum in *Mathematica*.

For the simpler Schwarzschild problem, the same basic procedure was first implemented in [62], where the (first-order BHPT) redshift invariant was expanded to 6.5PN and  $e^2$  in eccentricity and to 4PN and  $e^4$ . This was quickly extended by [27] to 4PN through  $e^{10}$ . Later, the authors of [32] improved the eccentric knowledge to 9.5PN and  $e^8$ , as that level was needed to complete a novel transcription of the redshift invariant to the scattering angle for hyperbolic orbits, which can be used to compute the full post-Minkowskian dynamics to high order. Finally, our previous work [20] brought the eccentric Schwarzschild expansion

to 10PN and  $e^{20}$ . Interestingly, by taking the expansions to such high order in e, we were able to find many PN terms which could be manipulated into either closed-form expressions or infinite series with known coefficients, following similar developments in the fluxes [15–17,84]. In fact, it was discovered that the entire leading logarithm series of the energy flux at infinity [15,17] exactly reappears in the redshift invariant.

This paper now extends many of those same advances to the more difficult Kerr problem, which has historically seen much less development. The first expansion for eccentric, equatorial orbits was undertaken in [53], finding a result to  $8.5\text{PN}/\mathcal{O}(e^2)/\mathcal{O}(a^2)$  in both a small-e and small-a limit. This was later extended to  $8.5\text{PN}/\mathcal{O}(e^4)/\mathcal{O}(a^2)$  in [54], which also derived an expression to 3.5PN and  $\mathcal{O}(a^2)$  using the full PN theory (i.e., for arbitrary mass ratio). We use the techniques and simplifications discussed in earlier sections of this paper to enhance these calculations greatly to the level of 6PN/e<sup>16</sup> and 8PN/e<sup>10</sup>, all while remaining exact in a. We then apply many of the techniques developed in the Schwarzschild case to extract closed-form eccentricity functions for the certain spin-dependent parts of the series. Note that in the expressions presented below, we redefine a to be dimensionless (i.e.,  $a \rightarrow a/M = \tilde{a}$ ) for simplicity.

## B. PN expansion of the redshift invariant

For eccentric, equatorial orbits, the first-order BHPT part of the generalized redshift invariant is found to take the following form, mirroring its circular-orbit limit [20,51]:

$$\langle u^{t} \rangle_{\tau}^{1} = \left( \frac{\mu}{M} \right) \frac{1}{p} \left[ \mathcal{U}_{0} + \frac{\mathcal{U}_{1}}{p} + \frac{\mathcal{U}_{3/2}}{p^{3/2}} + \frac{\mathcal{U}_{2}}{p^{2}} + \frac{\mathcal{U}_{5/2}}{p^{5/2}} + \frac{\mathcal{U}_{3}}{p^{3}} + \frac{\mathcal{U}_{7/2}}{p^{7/2}} + \left( \mathcal{U}_{4} + \mathcal{U}_{4L} \log p \right) \frac{1}{p^{4}} + \frac{\mathcal{U}_{9/2}}{p^{9/2}} + \left( \mathcal{U}_{5} + \mathcal{U}_{5L} \log p \right) \frac{1}{p^{5}} + \left( \mathcal{U}_{11/2} + \mathcal{U}_{11/2L} \log p \right) \frac{1}{p^{11/2}} + \left( \mathcal{U}_{6} + \mathcal{U}_{6L} \log p \right) \frac{1}{p^{6}} + \left( \mathcal{U}_{13/2} + \mathcal{U}_{13/2L} \log p \right) \frac{1}{p^{13/2}} + \left( \mathcal{U}_{7} + \mathcal{U}_{7L} \log p + \mathcal{U}_{7L2} \log^{2} p \right) \frac{1}{p^{7}} + \frac{\mathcal{U}_{15/2}}{p^{15/2}} + \left( \mathcal{U}_{8} + \mathcal{U}_{8L} \log p + \mathcal{U}_{8L2} \log^{2} p \right) \frac{1}{p^{8}} + \cdots \right]. \tag{5.5}$$

Note that we restore use of the parameter  $1/p = v^2$  in this section, as it is more commonly used in the literature. This expansion exhibits two key differences from its Schwarzschild counterpart. The first is that while in the Schwarzschild limit each term  $\mathcal{U}_i$  was a function of eccentricity alone, now each  $\mathcal{U}_i = \mathcal{U}_i(a,e)$  is a function of both eccentricity e and spin a. In many cases we will be able to extract their exact dependence on both parameters, though often our results will be Taylor expanded in e. The second is the presence of half-integer terms starting at the 1.5PN level. These terms are purely spin dependent, as the first half-integer PN term in the nonspinning case appears at 5.5PN.

In this work, we present only the spin-dependent coefficients, as the a=0 limit was discussed at length in [20]. To support this effort, we define an additional layer of specification at each order,

$$\mathcal{U}_i(a,e) = \mathcal{U}_i(e)^{\mathrm{Sch}} + \sum_{k=0} a^k \mathcal{U}_i(a,e)^{Sk}, \quad (5.6)$$

such that the first term  $U_i(e)^{\text{Sch}}$  corresponds to the Schwarzschild limit, and the superscript k describes the power of a attached to the remaining functions. All terms through 6PN were found through  $e^{16}$  (if not exactly), while

the orders 6.5PN–8PN were found to  $e^{10}$ . Some of the functions at higher orders are too lengthy to display in their entirety. These are truncated after a few eccentricity coefficients; however, we add a Greek letter (e.g.,  $\alpha_{16}$ ) to the end of such functions to remind the reader of the extent of the series. The full results are made available in

electronic form on the black hole perturbation toolkit [60], as well as the UNC gravity repository [61].

We begin with the functions through 3.5PN order, which all yield closed-form expressions. The first two terms are entirely spin independent, so we list the spin-dependent enhancement functions from 1.5PN-3.5PN:

$$\mathcal{U}_{3/2}^{S1} = -2(1 - e^2)^2 + 5(1 - e^2)^{3/2},$$

$$\mathcal{U}_{2}^{S2} = (1 - e^2)^2 - 2(1 - e^2)^{3/2},$$

$$\mathcal{U}_{5/2}^{S2} = (1 - e^2)^2(-20 + 8e^2) + (1 - e^2)^{3/2}(38 + 5e^2),$$

$$\mathcal{U}_{3}^{S2} = (1 - e^2)^2(13 - e^2) - (1 - e^2)^2(27 + 29e^2),$$

$$\mathcal{U}_{7/2}^{S1} = (1 - e^2)^2 \left(-\frac{87}{2} - \frac{93e^2}{2} + 30e^4\right) + (1 - e^2)^{3/2} \left(\frac{261}{2} + \frac{1195e^2}{4} - \frac{581e^4}{8}\right),$$

$$\mathcal{U}_{7/2}^{S3} = -2(1 - e^2)^2(1 + e^2) + (1 - e^2)^{3/2} \left(5 + \frac{37e^2}{2}\right).$$
(5.7)

Note that any functions not explicitly referenced (both here and throughout this section), such as  $\mathcal{U}_3^{S1}$  or  $\mathcal{U}_{7/2}^{S2}$ , are identically 0. At 4PN order, the spin-independent portion becomes more complicated [20]; however, the spin dependence remains simple:

$$\mathcal{U}_{4}^{S2} = (1 - e^{2})^{2} (52 + 63e^{2} - 35e^{4}) + (1 - e^{2})^{3/2} \left( -155 - \frac{1095e^{2}}{2} + 21e^{4} \right),$$

$$\mathcal{U}_{4}^{S4} = -3(1 - e^{2})^{3/2}e^{2}.$$
(5.8)

The 4.5PN functions can also be put into exact form, though with the first appearance of a transcendental coefficient:

$$\mathcal{U}_{9/2}^{S1} = (1 - e^2)^2 (-128 - 156e^2 - 28e^4 + 32e^6) + (1 - e^2)^{3/2} \left(\frac{5042}{9} - \frac{241\pi^2}{96} + \left(2699 - \frac{405\pi^2}{32}\right)e^2 + \left(\frac{1625}{12} - \frac{569\pi^2}{256}\right)e^4 - \frac{1447e^6}{8}\right),$$

$$\mathcal{U}_{9/2}^{S3} = (1 - e^2)^2 (-55 + 3e^2 + 12e^4) + (1 - e^2)^{3/2} \left(105 + \frac{867e^2}{2} + \frac{309e^4}{4}\right). \tag{5.9}$$

The 5PN functions likewise resemble their 4.5PN counterparts above, involving factors of  $\pi^2$ :

$$\mathcal{U}_{5}^{S2} = (1 - e^{2})^{2} \left( \frac{1099}{2} - 420e^{2} + \frac{879e^{4}}{2} - 121e^{6} \right) + (1 - e^{2})^{3/2} \left( -\frac{7067}{6} + \frac{593\pi^{2}}{512} + \left( -\frac{60485}{12} + \frac{3091\pi^{2}}{512} \right) e^{2} + \left( -\frac{4697}{3} + \frac{4403\pi^{2}}{4096} \right) e^{4} + \frac{3689e^{6}}{8} \right),$$

$$\mathcal{U}_{5}^{S4} = (1 - e^{2})^{2} (45 - 46e^{2} + e^{4}) + (1 - e^{2})^{3/2} \left( -53 - \frac{319e^{2}}{2} - \frac{127e^{4}}{2} \right). \tag{5.10}$$

The 5.5PN term  $U_{11/2}^{S1}$  marks the first appearance of additional transcendental numbers ( $\gamma_E$ , log 2, etc.), as well as a log p term with spin dependence. As might be expected from the Schwarzschild case, this is the first term for which we cannot determine a closed or exact function in eccentricity and must rely on the Taylor expansion through  $e^{16}$ . However, we can factor this term into a simpler form reminiscent of  $U_4^{\text{Sch}}$  [20], in order to capture some of the transcendental dependence.

We present the infinite series portion of  $U_{11/2}^{S1}$  to  $e^8$ , saving the full results for the online repositories [60,61]. The remaining enhancement functions are closed in form:

$$\begin{split} \mathcal{U}_{11/2}^{S1} &= \pi^2 (1 - e^2)^{3/2} \left( -\frac{79573}{768} - \frac{50411e^2}{128} - \frac{166217e^4}{2048} + \frac{4681e^6}{6144} \right) - 2 \left[ \gamma_E + \log \left( \frac{8}{1 + \sqrt{1 - e^2}} \right) \right] \mathcal{U}_{11/2L}^{S1} \\ &+ (1 - e^2)^{3/2} \left[ \left( \frac{1163681}{450} - \frac{32 \log(2)}{15} \right) + \left( \frac{6101333}{300} - \frac{45296 \log(2)}{15} + 2916 \log(3) \right) e^2 \right. \\ &+ \left( \frac{124628}{75} + \frac{729956 \log(2)}{15} - \frac{285039 \log(3)}{10} \right) e^4 \\ &+ \left( -\frac{25544941}{7200} - \frac{17042578 \log(2)}{45} + \frac{1805733 \log(3)}{16} + \frac{12578125 \log(5)}{144} \right) e^6 \\ &+ \left( -\frac{61976903}{46080} + \frac{45460366 \log(2)}{27} + \frac{181311291 \log(3)}{2560} - \frac{10682734375 \log(5)}{13824} \right) e^8 + \dots + \alpha_{16}e^{16} + \mathcal{O}(e^{18}) \right], \\ \mathcal{U}_{11/2}^{S3} &= (1 - e^2)^2 \left( -\frac{2399}{2} + \frac{5001e^2}{4} - \frac{1843e^4}{4} + 130e^6 \right) + (1 - e^2)^{3/2} \left( \frac{3289}{2} + \frac{11323e^2}{2} + \frac{42641e^4}{16} - \frac{4749e^6}{16} \right), \\ \mathcal{U}_{11/2}^{S5} &= (1 - e^2)^2 \left( -\frac{39}{2} + \frac{47e^2}{2} \right) + (1 - e^2)^{3/2} \left( \frac{39}{2} + \frac{131e^2}{4} + \frac{27e^4}{2} \right), \\ \mathcal{U}_{11/2L}^{S1} &= -(1 - e^2)^{3/2} \left( \frac{1168}{15} + \frac{6584e^2}{15} + \frac{1898e^4}{5} + \frac{491e^6}{15} \right). \end{aligned} \tag{5.11}$$

At 6PN order we find an analogous set of functions. Again, we truncate the more complicated series at  $e^8$ , leaving the full functions for the online repositories. The remaining functions are likewise found to yield closed forms:

$$\begin{split} \mathcal{U}_{6}^{S2} &= \pi^{2} (1 - e^{2})^{3/2} \left[ \frac{67439}{3072} + \frac{350857e^{2}}{2048} + \frac{1564717e^{4}}{8192} + \frac{975293e^{6}}{49152} + \left( -\frac{287}{32} - \frac{287e^{2}}{64} \right) (1 - e^{2})^{3/2} \right] \\ &- 2 \left[ \gamma_{E} + \log \left( \frac{8}{1 + \sqrt{1 - e^{2}}} \right) \right] \mathcal{U}_{6L}^{S2} + (1 - e^{2})^{3/2} \left[ \left( -\frac{741686}{225} + \frac{8 \log(2)}{5} \right) \right. \\ &+ \left( -\frac{4131994}{75} + \frac{4508 \log(2)}{5} - \frac{4374 \log(3)}{5} \right) e^{2} + \left( -\frac{1275121}{75} - \frac{193109 \log(2)}{15} + \frac{296703 \log(3)}{40} \right) e^{4} \\ &+ \left( \frac{599647}{200} + \frac{7664441 \log(2)}{90} - \frac{3812427 \log(3)}{160} - \frac{6015625 \log(5)}{288} \right) e^{6} \\ &+ \left( \frac{2004023}{2560} - \frac{1426452 \log(2)}{5} - \frac{310330197 \log(3)}{10240} + \frac{880390625 \log(5)}{6144} \right) e^{8} + \dots + \beta_{16}e^{16} + \mathcal{O}(e^{18}) \right], \\ \mathcal{U}_{6}^{S4} &= (1 - e^{2})^{2} (1444 - 1347e^{2} - 47e^{4} - 50e^{6}) + (1 - e^{2})^{3/2} \left( -1600 - 4386e^{2} - 1908e^{4} - \frac{339e^{6}}{4} \right), \\ \mathcal{U}_{6}^{S6} &= 3(1 - e^{2})^{3} + (1 - e^{2})^{3/2} \left( -3 - \frac{9e^{2}}{2} \right), \\ \mathcal{U}_{6L}^{S2} &= (1 - e^{2})^{3/2} \left( \frac{132}{5} + \frac{718e^{2}}{5} + \frac{293e^{4}}{2} + \frac{883e^{6}}{60} \right). \end{aligned}$$
 (5.12)

From 6.5PN through 8PN, our expansion is limited to order  $e^{10}$  in eccentricity, which greatly reduces our ability to determine closed-form expressions from the series. From here, we primarily present just the first few coefficients in each function. Again, the full results are posted at the repositories [60,61]. The 6.5PN term marks the first appearance of the polygamma function. We set  $\psi^{(n,k)} = \psi^{(n)}(\frac{ika}{\kappa}) + \psi^{(n)}(-\frac{ika}{\kappa})$  for polygamma function  $\psi^{(n)}(x)$  and find

$$\begin{split} \mathcal{U}_{13/2}^{S1} &= -\frac{1}{3}(1-e^2)^{3/2} \bigg( \log \kappa - \gamma_E + \frac{1}{2} \psi^{(0,2)} \bigg) \mathcal{U}_{13/2L}^{S3} - 2 \bigg[ \gamma_E + \log \bigg( \frac{8}{1+\sqrt{1-e^2}} \bigg) \bigg] \mathcal{U}_{13/2L}^{S1} \\ &+ (1-e^2)^{3/2} \bigg[ \bigg( \frac{137967017}{4410} - \frac{2648651\pi^2}{1024} - \frac{1528\log(2)}{5} + \frac{1944\log(3)}{7} \bigg) + \bigg( \frac{3227202952}{11025} - \frac{27517957\pi^2}{1536} \bigg) \\ &+ \frac{88816\log(2)}{15} + \frac{5346\log(3)}{7} \bigg) e^2 + \bigg( \frac{4589364091}{29400} - \frac{146807929\pi^2}{12288} - \frac{6151762\log(2)}{35} - \frac{5423031\log(3)}{140} \bigg) \\ &+ \frac{5859375\log(5)}{56} \bigg) e^4 + \dots + \gamma_{10}e^{10} + \mathcal{O}(e^{12}) \bigg], \\ \mathcal{U}_{13/2}^{S3} &= -(1-e^2)^{3/2} \bigg( \log 2\kappa + \gamma_E + \frac{1}{2} \psi^{(0,2)} \bigg) \mathcal{U}_{13/2L}^{S3} + (1-e^2)^{3/2} \bigg[ \bigg( \frac{696161}{225} - \frac{115\pi^2}{96} \bigg) + \bigg( \frac{1731571}{18} - \frac{38825\pi^2}{768} \bigg) e^2 \\ &+ \bigg( \frac{776917}{24} - \frac{17911\pi^2}{512} \bigg) e^4 + \bigg( -\frac{119507}{48} - \frac{3483\pi^2}{2048} \bigg) e^6 + \bigg( -\frac{162431}{256} + \frac{861\pi^2}{2048} \bigg) e^8 \\ &+ \bigg( -\frac{47309}{1600} + \frac{369\pi^2}{2048} \bigg) e^{10} + \mathcal{O}(e^{12}) \bigg], \\ \mathcal{U}_{13/2L}^{S5} &= (1-e^2)^{3/2} \bigg( \frac{102}{5} + 3694e^2 + \frac{2503e^4}{4} - \frac{333e^6}{8} - \frac{6157e^8}{128} - \frac{345e^{10}}{16} + \mathcal{O}(e^{12}) \bigg), \\ \mathcal{U}_{13/2L}^{S3} &= -(1-e^2)^{3/2} \bigg( \frac{18268}{105} + \frac{31008e^2}{35} + \frac{72857e^4}{105} + \frac{2118e^6}{7} + \frac{62603e^8}{1120} \bigg), \\ \mathcal{U}_{13/2L}^{S3} &= -(1-e^2)^{3/2} \bigg( \frac{96}{5} + 144e^2 + 108e^4 + 6e^6 \bigg). \end{aligned}$$

The 7PN functions are similar in structure to their 6PN counterparts, though we do note the first appearance of an odd power of a at integer order. Additionally, we no longer have enough coefficients in the function S2 to identify any eccentric structure, so we simply present a few of those coefficients unmodified. We find

$$\mathcal{U}_{7}^{S1} = \pi (1 - e^2)^{3/2} \left( \frac{343088}{1575} + \frac{394122e^2}{175} + \frac{5969582e^4}{1575} + \frac{661759039e^6}{453600} + \frac{152835577e^8}{2419200} + \frac{246822697e^{10}}{290304000} + \mathcal{O}(e^{12}) \right)$$

$$\mathcal{U}_{7}^{S2} = (1 - e^2)^{3/2} \left[ \left( \frac{15442453}{3150} - \frac{74024\gamma_E}{105} - \frac{193510709\pi^2}{98304} - \frac{27016\log(2)}{21} - \frac{729\log(3)}{7} \right) + \left( -\frac{633681119}{2100} - \frac{685264\gamma_E}{105} \right) \right]$$

$$- \frac{736121519\pi^2}{49152} + \frac{322384\log(2)}{35} - \frac{785376\log(3)}{35} \right) e^2 + \left( -\frac{140377429}{1680} - \frac{1019254\gamma_E}{105} - \frac{4127285485\pi^2}{393216} \right)$$

$$- \frac{46263526\log(2)}{105} + \frac{327468987\log(3)}{1120} - \frac{21484375\log(5)}{672} \right) e^4 + \dots + \delta_{10}e^{10} + \mathcal{O}(e^{12}) \right]$$

$$\mathcal{U}_{7}^{S4} = (1 - e^2)^{3/2} \left[ \left( -\frac{4900}{3} - \frac{69\pi^2}{256} \right) + \left( -115532 + \frac{585\pi^2}{64} \right) e^2 + \left( -\frac{313281}{8} + \frac{10521\pi^2}{2048} \right) e^4 \right]$$

$$+ \left( \frac{129643}{48} - \frac{267\pi^2}{2048} \right) e^6 + \left( \frac{119151}{128} - \frac{861\pi^2}{8192} \right) e^8 + \left( \frac{108689}{256} - \frac{369\pi^2}{8192} \right) e^{10} + \mathcal{O}(e^{12}) \right],$$

$$\mathcal{U}_{7}^{S6} = (1 - e^2)^{3/2} \left( -1374e^2 - \frac{2145e^4}{16} + \frac{1671e^6}{32} + \frac{5055e^8}{256} + \frac{4401e^{10}}{512} + \mathcal{O}(e^{12}) \right),$$

$$\mathcal{U}_{7L}^{S6} = (1 - e^2)^{3/2} \left( \frac{37012}{105} + \frac{342632e^2}{105} + \frac{509627e^4}{105} + \frac{206029e^6}{105} + \frac{27501e^8}{224} - \frac{2303e^{10}}{240} + \mathcal{O}(e^{12}) \right).$$

The 7.5PN functions S1 and S3 show interesting behavior, in that they present certain transcendental numbers attached to (apparently) terminating series that do not bear any obvious relationship to the corresponding logarithmic functions:

$$\mathcal{U}_{15/2}^{S1} = (1-e^2)^{3/2} \left[ \left( \frac{224}{5} + \frac{2448e^2}{5} + 708e^4 + 182e^6 + \frac{9e^8}{2} \right) \log \kappa + \left( \frac{16}{5} + \frac{224e^2}{5} + 84e^4 + 28e^6 + \frac{7e^8}{8} \right) \psi^{(0,1)} \right. \\ + \left( \frac{96}{5} + 200e^2 + 270e^4 + 63e^6 + \frac{11e^8}{8} \right) \psi^{(0,2)} + \left( \frac{8776579}{32768} + \frac{653303597e^2}{262144} + \frac{2529471329e^4}{1048576} + \frac{174272943e^6}{2097152} \right. \\ - \frac{317401461e^8}{16777216} \right) \pi^4 \right] + (1-e^2)^{3/2} \left[ \left( \frac{630173174963}{3572100} - \frac{2026048\gamma_E}{2835} - \frac{15709506835\pi^2}{884736} - \frac{259648\log(2)}{2835} \right. \\ - \frac{5832\log(3)}{7} \right) + \left( \frac{6701813671607}{2381400} - \frac{889124\gamma_E}{81} - \frac{97156196179\pi^2}{442368} - \frac{429451756\log(2)}{2835} + \frac{5378319\log(3)}{140} \right. \\ + \frac{9765625\log(5)}{324} \right) e^2 + \dots + \epsilon_{10}e^{10} + \mathcal{O}(e^{12}) \right], \\ \mathcal{U}_{15/2}^{S2} = \pi(1-e^2)^{3/2} \left[ \left( \frac{552}{5} + \frac{5664e^2}{105} - \frac{81213e^2}{175} - \frac{1577929e^4}{1800} - \frac{5597705e^6}{12096} - \frac{9631177e^8}{387072} - \frac{1386265357e^{10}}{2993040000} + \mathcal{O}(e^{12}) \right), \\ \mathcal{U}_{15/2}^{S3} = (1-e^2)^{3/2} \left[ \left( \frac{552}{5} + \frac{5664e^2}{105} + 1494e^4 + 336e^6 + \frac{111e^8}{16} \right) \log \kappa - \left( \frac{12}{5} + \frac{168e^2}{5} + 63e^4 + 21e^6 + \frac{21e^8}{32} \right) \psi^{(0,1)} \right. \\ + \left. \left( \frac{288}{5} + 600e^2 + 810e^4 + 189e^6 + \frac{33e^8}{8} \right) \psi^{(0,2)} \right] + (1-e^2)^{3/2} \left[ \left( \frac{5268133}{225} + \frac{6488\gamma_E}{15} - \frac{3298493\pi^2}{6144} \right) \right. \\ + \frac{11096\log(2)}{15} \right) + \left( \frac{246222767}{225} + \frac{68968\gamma_E}{15} - \frac{4438835\pi^2}{768} - 6120\log(2) + \frac{64152\log(3)}{5} \right) e^2 \\ + \dots + \xi_{10}e^{10} + \mathcal{O}(e^{12}) \right], \\ \mathcal{U}_{15/2}^{S7} = (1-e^2)^{3/2} \left( \frac{2251}{5} + \frac{490316e^2}{5} + \frac{64077e^4}{16} - \frac{53317e^6}{256} - \frac{605545e^8}{512} - \frac{325199e^{10}}{512} + \mathcal{O}(e^{12}) \right), \\ \mathcal{U}_{15/2L}^{S7} = (1-e^2)^{3/2} \left( \frac{189904}{567} + \frac{2123666e^2}{16} + \frac{849e^8}{2835} - \frac{11e^{10}}{1890} + \frac{329151e^8}{280} - \frac{5671807e^{10}}{20160} + \mathcal{O}(e^{12}) \right), \\ \mathcal{U}_{15/2L}^{S3} = (1-e^2)^{3/2} \left( \frac{189904}{567} + \frac{2123666e^2}{405} + \frac{52036532e^4}{2835} + \frac{27140887e^6}{1890} + \frac{329151e^8}{40} - \frac{5671807e^{10}}{20160} + \mathcal{O}(e^{12}) \right), \\ \mathcal{U}_{15/2L}^{S3} = (1-e^2)^{3/2} \left( \frac{4072}{5} + \frac{8896e^2}$$

Finally, the 8PN functions introduce several elements of additional new structure. One is in the form of a spin-dependent term  $\mathcal{U}_8^{S0}$  with no leading factor of a. The attached eccentricity series for both  $\mathcal{U}_8^{S0}$  and  $\mathcal{U}_8^{S3}$  appear to terminate at  $e^8$ , so they are presented in their entirety, while the (apparently infinite) series  $\mathcal{U}_8^{S1}$ ,  $\mathcal{U}_8^{S2}$ , and  $\mathcal{U}_8^{S4}$  are truncated for brevity. Additionally, we find the appearance of a second polygamma combination, commonly denoted  $\bar{\psi}^{(n,k)} = -i(\psi^{(n)}(\frac{ika}{\kappa}) - \psi^{(n)}(-\frac{ika}{\kappa}))$ , as well of  $\kappa$  in the denominators of certain coefficients. The full results begin

$$\begin{split} \mathcal{U}_{8}^{S0} &= (1-e^{2})^{3/2} \bigg[ \bigg( \frac{1712}{525} - \frac{64\gamma_{E}}{5} + \frac{1712\kappa}{525} - \frac{32\psi^{(0,2)}}{5} - \frac{64\log(\kappa)}{5} \bigg) + \bigg( \frac{26536}{525} - \frac{968\gamma_{E}}{5} + \frac{25252\kappa}{525} - \frac{484\psi^{(0,2)}}{5} \bigg) \\ &- \frac{992\log(\kappa)}{5} \bigg) e^{2} + \bigg( \frac{3638}{35} - 390\gamma_{E} + \frac{3317\kappa}{35} - 195\psi^{(0,2)} - 408\log(\kappa) \bigg) e^{4} + \bigg( \frac{3959}{105} - 139\gamma_{E} + \frac{1391\kappa}{42} - \frac{139\psi^{(0,2)}}{2} \bigg) \\ &- 148\log(\kappa) \bigg) e^{6} + \bigg( \frac{107}{84} - \frac{37\gamma_{E}}{8} + \frac{1819\kappa}{1680} - \frac{37\psi^{(0,2)}}{16} - 5\log(\kappa) \bigg) e^{8} \bigg], \\ \mathcal{U}_{8}^{S1} &= (1 - e^{2})^{3/2} \bigg[ \bigg( \frac{2389021\pi}{9450} - \frac{3424\bar{\psi}^{(0,2)}}{525} - \frac{192\kappa\bar{\psi}^{(1,2)}}{5} + \frac{256\bar{\psi}^{(1,2)}}{5\kappa} \bigg) \\ &+ \bigg( -\frac{108802823\pi}{132300} - \frac{51788\bar{\psi}^{(0,2)}}{525} - \frac{2904\kappa\bar{\psi}^{(1,2)}}{5} + \frac{3872\bar{\psi}^{(1,2)}}{5\kappa} \bigg) e^{2} + \dots + \chi_{10}e^{10} + \mathcal{O}(e^{12}) \bigg], \end{split}$$

$$\mathcal{U}_8^{S2} = (1-e^2)^{3/2} \left[ \left( \frac{75054389639}{198450} - \frac{1753576\gamma_E}{567} + \frac{1712\kappa}{175} - \frac{314206240595\pi^2}{7077888} - \frac{417436343\pi^4}{16777216} - \frac{64\psi^{(0.1)}}{15} \right. \\ \left. - \frac{432\psi^{(0.2)}}{5} - \frac{14672264\log(2)}{2835} - 972\log(3) - \frac{544\log(\kappa)}{3} \right) + \left( \frac{29407415438}{14175} - \frac{3574292\gamma_E}{81} + \frac{26322\kappa}{175} \right. \\ \left. - \frac{8172744049193\pi^2}{14155776} - \frac{1047412729\pi^4}{4194304} - \frac{896\psi^{(0.1)}}{15} - 1276\psi^{(0.2)} + \frac{134696372\log(2)}{2835} - \frac{36823977\log(3)}{280} \right. \\ \left. - \frac{48828125\log(5)}{4536} - \frac{39928\log(\kappa)}{15} \right) e^2 + \dots + h_{10}e^{10} + \mathcal{O}(e^{12}) \right], \\ \mathcal{U}_8^{S3} = (1-e^2)^{3/2} \left[ -\frac{3424\bar{\psi}^{(0.2)}}{175} - \frac{51788\bar{\psi}^{(0.2)}e^2}{175} - \frac{4173\bar{\psi}^{(0.2)}e^4}{7} - \frac{14873\bar{\psi}^{(0.2)}e^6}{70} - \frac{3959\bar{\psi}^{(0.2)}e^8}{560} \right], \\ \mathcal{U}_8^{S4} = (1-e^2)^{3/2} \left[ \left( -\frac{2910653}{225} - \frac{584\gamma_E}{5} + \frac{269059\pi^2}{98304} + \frac{16\psi^{(0.1)}}{5} - 48\psi^{(0.2)} - \frac{712\log(2)}{5} - \frac{448\log(\kappa)}{5} \right) \right. \\ \left. + \left( -\frac{81173087}{50} - 1624\gamma_E - \frac{214\kappa}{175} + \frac{9737469\pi^2}{16384} + \frac{224\psi^{(0.1)}}{5} - \frac{3168\psi^{(0.2)}}{5} - \frac{464\log(2)}{5} - \frac{8748\log(3)}{5} \right. \\ \left. - \frac{5912\log(\kappa)}{5} \right) e^2 + \dots + q_{10}e^{10} + \mathcal{O}(e^{12}) \right], \\ \mathcal{U}_8^{S6} = (1-e^2)^{3/2} \left( -\frac{249}{5} - \frac{293474e^2}{5} - 17592e^4 + \frac{12229e^6}{32} + \frac{268889e^8}{256} + \frac{121663e^{10}}{256} + \mathcal{O}(e^{12}) \right), \\ \mathcal{U}_8^{S8} = (1-e^2)^{3/2} \left( \frac{228196}{567} + \frac{9472814e^2}{405} + \frac{192633277e^4}{5670} + \frac{86757829e^6}{11340} + \frac{22396051e^8}{10080} + \frac{3088957e^{10}}{10080} + \mathcal{O}(e^{12}) \right), \\ \mathcal{U}_{8L}^{S4} = (1-e^2)^{3/2} \left( \frac{516}{5} + \frac{7028e^2}{405} + \frac{192633277e^4}{155} + \frac{16568e^6}{15} + \frac{21739e^8}{480} - \frac{329e^{10}}{160} + \mathcal{O}(e^{12}) \right).$$

## C. Discussion

When PN expansions are made in the extreme-mass-ratio limit using the Teukolsky-MST formalism described in this paper, the result is a double Taylor series about 1/p = 0and e = 0, taken to finite orders in both parameters. Nevertheless, significant prior work at the intersection of BHPT and PN theory in the Schwarzschild limit has revealed that the derived terms should have significant structure in their dependence on eccentricity. Direct derivations from the full PN theory, for instance, have found closed-form expressions (or fully understood infinite series) for the first three orders in the energy flux and the redshift invariant [48,85–87]. Likewise, work has been done to characterize the behavior of eccentricity enhancement functions as e approaches 1, again in the Schwarzschild limit [16,84,88]. Our knowledge of the underlying PN structure can then be used to refactor the initial (Taylor series) results into the corresponding exact functions of eccentricity that would produce those series, greatly enhancing our access to the high-e regime.

In the Schwarzschild case, this effort proved highly effective, as BHPT-PN expansions were found to yield a

great many closed forms in the fluxes [15,17–19], redshift invariant [20], and spin-precession invariant [21]. With the success of those methods in hand, we were motivated to push the eccentric expansion in the Kerr regime, to see if similar structure would appear in the spin dependence of the PN expansion. We first confirmed some of the same structure in the fluxes at infinity [40], and with this work we now see that many of the patterns repeat in the redshift invariant, though not without significant added complexity and a few unexpected irregularities. We review the results here.

The first eight PN functions,  $\mathcal{U}_{3/2}$ ,  $\mathcal{U}_2$ ,  $\mathcal{U}_{5/2}$ ,  $\mathcal{U}_3$ ,  $\mathcal{U}_{7/2}$ ,  $\mathcal{U}_4$ ,  $\mathcal{U}_{9/2}$ , and  $\mathcal{U}_5$ , are all found to yield straightforward closed forms. When separated by power of a, we find that each takes the form of a pair of polynomials in e, each attached to a factor of  $(1-e^2)$  to some positive power. [Recall that when  $y=(M\Omega_{\varphi})^{2/3}$  is used as the PN expansion parameter instead of 1/p, the factors of  $(1-e^2)$  carry negative powers, commonly called eccentricity singular factors [15,84].] These functions are all vaguely reminiscent of the 2PN energy flux [86], which was the first derived PN term to display a similar combination of

polynomials attached to differing eccentricity singular factors.

Using the Schwarzschild limit as a model, it could perhaps be predicted that these functions would be compact, as the first term there with a nontrivial structure was  $\mathcal{U}_4^{\text{Sch}}$ . Thus, we might expect that the first nontrivial term in the spinning case would be four orders after the first, at 5.5PN order. Nevertheless, it is remarkable that the spin dependence (at least in the equatorial limit) can be known exactly up to that point. Additionally, the only term in the Schwarzschild limit not fully understood to this level is  $\mathcal{U}_5^{\text{Sch}}$ , as it has a dependence on the 1PN multipole moments that has not yet been elucidated (see [20] for more details). Once that piece is determined, the entire 5PN redshift invariant will be understood for eccentric equatorial EMRIs on a Kerr background.

The 5.5PN function  $\mathcal{U}_{11/2}^{S1}$  carries the first major increase in coefficient complexity, presenting a form that resembles  $\mathcal{U}_4^{\text{Sch}}$ . Given the similarity, and based on prior work in the Schwarzschild limit [17,20], we would expect the log coefficients in this term to stem from a  $\chi(e)$ -like enhancement function (see [86,87,89]), meaning they cannot be condensed into closed form. Nevertheless, if this is the case, such a function would likely yield to a derivation in terms of multipole moments, which could be expanded to arbitrary order in eccentricity. Indeed, this was precisely found to be the case for  $\mathcal{U}_4^{\text{Sch}}$  [20]. Despite a structure identical to that of  $\mathcal{U}_{11/2}^{\text{Sch}}$ , knowledge of the multipolar composition of  $\mathcal{U}_4^{\text{Sch}}$  allows us to expand the function to arbitrary order in eccentricity.

Further bolstering support for this prospect is the fact that the 5.5PN log term  $\mathcal{U}_{11/2L}^{S1}$  is exactly proportional to the leading spin dependence of the energy flux  $\mathcal{L}_{3/2}^{S1}$  [40]. Curious connections between the energy flux series and redshift invariant series also appeared in the Schwarzschild limit [20]. In fact, we found that the entire leading logarithm series of the energy flux (that is, the first appearance of each new power of log p, including power 0—see [15]) recurred in the redshift invariant, but shifted four PN orders up. Indeed, the Peters-Mathews energy flux term was found to be proportional to  $\mathcal{U}_{4L}^{\mathrm{Sch}}.$  In this case we could not find an infinite sequence of PN terms with proportionality between the two, but the three terms  $\mathcal{U}_{11/2L}^{S1}$ ,  $\mathcal{U}_{6L}^{S2}$ , and  $\mathcal{U}_{15/2}^{S2}$  showed correspondence with  $\mathcal{L}_{3/2}^{S1}$ ,  $\mathcal{L}_{2}^{S2}$ , and  $\mathcal{L}_{7/2}^{S2}$ , respectively. Whether there is a deeper pattern there remains an open question and will be left to future investigation.

The next major increase in complexity occurs at 6.5PN order, with the functions  $\mathcal{U}_{13/2}^{S1}$  and  $\mathcal{U}_{13/2}^{S3}$ . We have used the limited number of coefficients to extract what seems to be the complete dependence of the polygamma,  $\log \kappa$ , and  $\gamma_E$  terms on the logarithmic functions  $\mathcal{U}_{13/2L}^{S1}$  and  $\mathcal{U}_{13/2L}^{S3}$ . The fact that both different logarithmic eccentricity functions

are present in the nonlogarithmic terms  $\mathcal{U}_{13/2}^{S1}$  is curious, and we conjecture that it represents the effect of a  $\kappa^2$  term on a combination of coefficients at an earlier stage of the derivation. The term  $\mathcal{U}_{13/2}^{S3}$  also exposes an additional irregularity, as it is the third PN order with an  $a^3$  dependence, meaning we would naively (following the pattern in the Schwarzschild, S1, and S2 functions) expect a series with no transcendentals other than  $\pi^2$ . However, we instead find further appearances of polygamma,  $\log \kappa$ , and  $\gamma_E$ , again possibly resulting from  $\kappa^2$  terms in the MST solutions.

At 7PN we see the first occurrence of an S1 function at an integer order. This function is attached to a factor of  $\pi$ , which is reminiscent of low-order tail terms in the energy flux. This makes sense, as the half-integer tail for the redshift invariant starts at 5.5PN in the Schwarzschild limit, and  $\mathcal{U}_{11/2}^{Sch}$  takes a very similar form to  $\mathcal{U}_7^{S1}.$  It is unlikely that this series terminates at finite order, but if its multipolar content resembles that of tail contributions to other observables like the fluxes, there may a route to an arbitrary-order expansion. The higher spin terms follow the same general structure as their counterparts at 6PN, though the lower range of the eccentricity expansion does not provide us with enough information to determine closed or exact functions. It is perhaps noteworthy that the 7PN functions are markedly simpler than their 6.5PN counterparts, showing no incidence of polygamma or  $\log \kappa$ . Additionally, the logarithmic term only contains one a function in  $\mathcal{U}_{7L}^{S2}$ , while  $\mathcal{U}_{13/2L}$  produced both S1 and S3.

There are a few interesting functions at 7.5PN order as well. In particular, in the functions S1 and S3, we find the transcendental terms  $\log \kappa$ ,  $\psi^{(0,1)}$ , and  $\psi^{(0,2)}$ , all attached to eccentricity series that appear to terminate at  $e^8$ . Moreover, the polynomials are linearly independent and bear no apparent relationship to the logarithmic functions  $\mathcal{U}_{15/2L}^{S1}$  and  $\mathcal{U}_{15/2L}^{S3}$ . As mentioned above, it is also noteworthy that the function  $\mathcal{U}_{15/2}^{S2}$ , the first appearance of an even power of a at half-integer order, shows the last connection to the energy flux expansion. Indeed the infinite eccentricity series is exactly proportional to the 3.5PN energy flux term  $\mathcal{L}_{7/2}^{S2}$ , though the more fundamental reason behind this particular connection remains unknown.

The final term at 8PN introduces another combinatorial increase in complexity. 8PN is the first order with a dependence in the term S0. In fact, this function appears to have terms that are independent of a and therefore belong in the Schwarzschild limit. However, it turns out that when the limit is taken  $a \to 0$ , these terms exactly cancel with polygamma terms that remain nonzero in  $\mathcal{U}_8^{S1}$ . Additionally, the term  $\mathcal{U}_8^{S0}$  appears to truncate at  $e^8$ . The functions S1 through S4 display similar behavior (though with varying degrees of complexity), while the remaining functions through  $\mathcal{U}_8^{S6}$ ,  $\mathcal{U}_{8L}^{S8}$ ,  $\mathcal{U}_{8L}^{S2}$ , and  $\mathcal{U}_{8L}^{S4}$  are rational

series. Broadly speaking, it appears the maximum power of a present in a given PN term tends to follow separate patterns for half-integer and integer orders. The half-integer orders follow the trend  $\{1,1,3,3,5,5...\}$ , while the integer orders follow the trend  $\{2,2,4,4,6,6,...\}$ . At each order, the higher powers of a tend to be rational, providing ample opportunity for the derivation of closed-form expressions.

#### D. Comparison to numerical data

We can assess the accuracy of these expansions by comparing them to the numerical calculations of the redshift invariant for specific values of p, e, and a. We evaluate orbits with  $p = \{10, 20\}$ ,  $e = \{1/10, 1/5\}$ , and  $a = \{1/4, 1/2, 9/10\}$  in an attempt to survey a range of parameters. The spin-independent portion of the expansion was more completely determined in [20], so we supplement

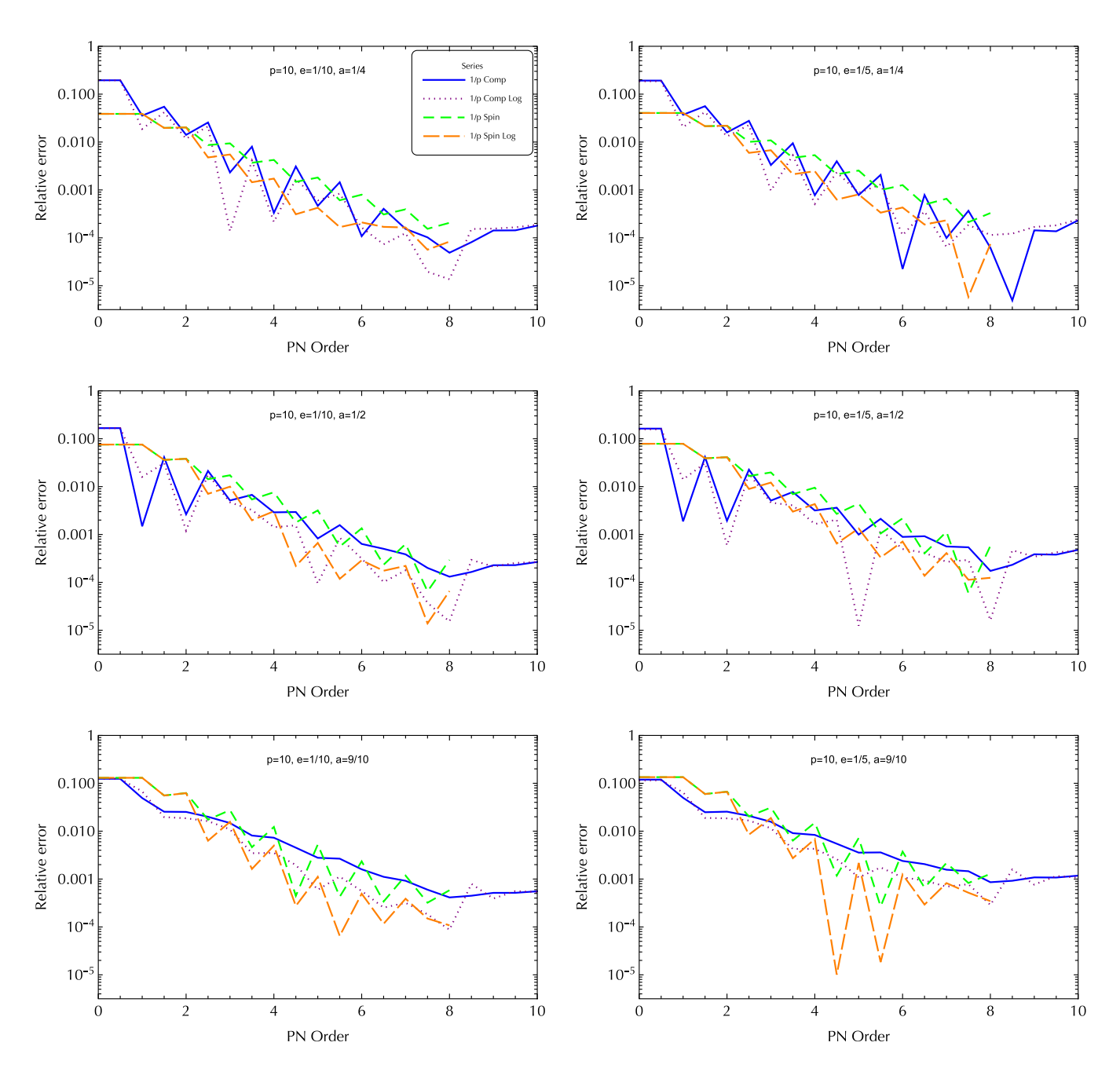


FIG. 1. Accuracy of the redshift invariant PN expansion and its resummations for several individual orbits. The numerical values of our redshift expansion are plotted against numerical calculations for several orbits with p = 10. Within each plot comparisons are made for a composite ("Comp") expansion against the full numerical redshift, as well as for the spin-dependent portion of the expansion against the redshift's spin-dependent residual, both with and without the use of the logarithmic summation. Numerical data was supplied by Zachary Nasipak. Lines in the plots level off when the expansion is accurate to within numerical error bounds.

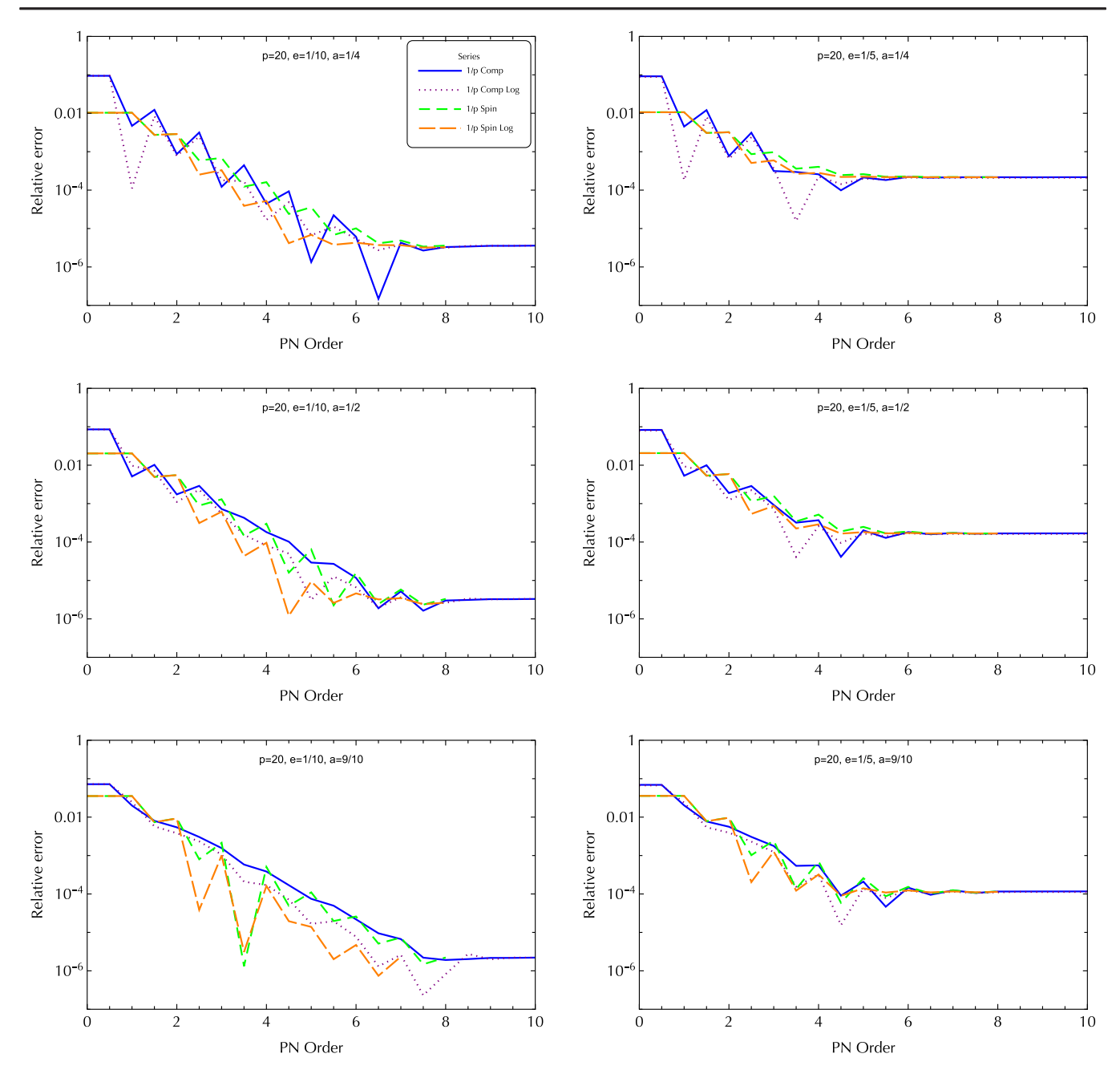


FIG. 2. Accuracy of the redshift invariant PN expansion and its resummations for p = 20. Numerical data was supplied by Zachary Nasipak. Lines in the plots level off when the expansion is accurate to within numerical error bounds (in particular, data points for p = 20, e = 1/5 were computed to lower accuracy, leading to earlier level off).

the current equatorial Kerr series with additional coefficients from [20] as needed. In order to better understand the behavior of the series, we make comparisons in two ways: (1) We construct a composite series, in which the spin-independent portion is supplied by the results in [20] to 10PN, and the spin-dependent portion from the present calculation is added through 8PN. (2) We use only the spin-dependent portion of the PN series, and we compare this to the residual numerical calculation found by subtracting the Schwarzschild redshift off the full Kerr value. Note that in

this case, the fractional error is still computed with respect to the full (Kerr) redshift value, not the difference. Finally, we try the logarithmic resummation of each method to check its effects on convergence [90,91]. These results are presented for p=10 in Fig. 1 and for p=20 in Fig. 2.

From the plots, we can see that the convergence follows a few trends across values of p, e, a, and PN order. The PN regime corresponds to larger p by definition, so the reduction in error from p=10 to p=20 matches expectations. The plots for the orbits with p=20, e=1/5 reach

the numerical error threshold around 6PN order, but we can still observe a steeper trend in these graphs than in their p=10 counterparts. Similarly, experience in the Schwarzschild limit [18,20] has revealed that the PN convergence tends to worsen with increasing e, which is generally reflected from the left to the right columns of the plots (though this fact is somewhat obscured by occasional irregular jumps).

What is perhaps most interesting is the apparent loss of convergence with increasing a. Higher values of a permit stable orbits with smaller values of p, so we might well expect higher a to improve convergence against the same value of p. Indeed, Ref. [92] noted a slight increase in series validity with a for low-order expansions of the energy flux in the circular-orbit limit. On the other hand, the expansion of the same quantity to 11PN in [37] revealed some erratic behavior at higher a, as the high-order terms began to reduce fidelity to numerical data in the strong field. The orbits presented here are farther from the innermost stable orbit than the relevant results in [37], so it is difficult to extrapolate from this the expected behavior of the redshift expansion. The worse performance observed at higher a (at least in these sample orbits) could be the result of an interaction with the eccentricity dependence (which is already known to reduce convergence [18,20]), or it could be a peculiar feature of the redshift or of the chosen orbits. It is also possible that the PN expansion is more broadly less convergent in the high spin regime. A clearer answer to this question requires deeper study, which will be left to future work.

Beyond these trends, we can note that each orbit with sufficient numerical accuracy shows monotonic improvement until around the 8PN level, at which point the spin dependence is lost. This fact implies that the Schwarzschild portion of the expansion, which remains from 8PN-10PN, is a poor substitute for the composite expansion. On the other hand, the steady improvement prior to that point implies that accuracy could continue to improve through the use of higher-order expansions. The present work to 8PN and  $e^{10}$  reached the limit of our supercomputing resources, with the bottleneck step requiring many parallelized jobs each lasting 8-10 days on the UNC supercomputing cluster Longleaf. Nevertheless, it would certainly be possible to extend the PN order at the expense of eccentricity, permitting an expansion to, say, 10PN and  $e^4$ . As usual, we should recall that the contributions to the orbital phase evolution by conservative terms are suppressed by the mass ratio relative to the flux [1], implying that even a slow-to-converge PN expansion of the conservative part of the self-force may be useful in close

Finally, we note that the comparison of the spin dependence alone against the residual difference between the Kerr redshift and the Schwarzschild redshift did not improve the convergence compared to the simple composite expansion. However, the residual expansion is very simple in form, so there may be a computational advantage to approaching the problem in this manner.

#### VI. CONCLUSIONS

This work has analytically derived the PN expansion of the generalized redshift invariant for eccentric, equatorial EMRIs with a Kerr primary to high order. The series is computed to 8PN and  $e^{10}$  in eccentricity, with the PN terms through 6PN found to  $e^{16}$ . Most importantly, each term in the expansion retained exact dependence on the spin parameter a, greatly advancing past work in the small-a limit [54]. The depth of the eccentricity expansion allows us to resum several eccentricity terms into closed-form expressions. Explicitly, exact expressions were found for the eccentricity dependence (and spin dependence) of the full terms  $\mathcal{U}_{3/2}$ ,  $\mathcal{U}_2$ ,  $\mathcal{U}_{5/2}$ ,  $\mathcal{U}_3$ ,  $\mathcal{U}_{7/2}$ ,  $\mathcal{U}_4$ ,  $\mathcal{U}_{9/2}$ ,  $\mathcal{U}_5$ ,  $\mathcal{U}_{11/2L}$ ,  $\mathcal{U}_{6L}$ ,  $\mathcal{U}_{13/2L}$ . Many additional eccentricity functions attached to individual powers of a were also found in closed form. Lastly, we restate the curious connection between the redshift terms  $\mathcal{U}_{11/2L}, \mathcal{U}_{6L}, \mathcal{U}_{15/2}^{S2}$  and counterpart terms in the energy flux [40]. The proportionality likely points to a common source of multipolar dependence, but the deeper significance of this connection will be left to future work. The full expansions can be found in the online repositories [60,61].

It is likely that with a deeper expansion in eccentricity, more terms with rational coefficients throughout the redshift series could be manipulated into closed form. However, for the purposes of transcribing these expansions into usable EOB models or waveform templates, the more important task lies in determining the multipolar dependence of  $\mathcal{U}_5^{\mathrm{Sch}}$  and then  $\mathcal{U}_{11/2}^{\mathrm{S1}}$ , as these are the last components with unknown contributions through 5.5PN order. Once such an understanding is developed, the full eccentricity and spin dependence of the redshift invariant series for Kerr equatorial EMRIs will be known through 5.5PN order. Note that the Schwarzschild limit of the redshift invariant was needed to 9.5PN and  $e^8$  to complete a useful derivation of the scattering angle to 6PN within a framework that combines PN theory, PM theory, and EOB theory, implying that these expansions continue to provide utility to high order [32]. Nevertheless, the extent of the relationship between BHPT-PN expansions in the Kerr case and the EOB Hamiltonian is still an active area of study [54].

By combining our results with the extended Schwarzschild expansions of [20], we were able to make comparisons to numerical results in Figs. 1 and 2, finding agreement to better than  $10^{-4}$  in most cases. We also discovered interesting trends in the asymptotic behavior of the series across values of p, e, and a. While the first two mostly followed expectations, the last showed a decreasing convergence with a that could point to a reduced efficacy of

the expansion in the high-spin regime. Further research into this question will be left to future work.

The techniques developed here can be utilized to expand the spin-precession invariant  $\psi$  for Kerr equatorial EMRIs [21,75,76]. This conservative quantity requires the expansion of the self-force, which involves first derivatives of the metric perturbations, along with the gauge portion of the metric completion piece [74,93]. In the Schwarzschild case, the spin-precession invariant incurred a factor of 5–10 greater computational expense, and the expansion process loses one order in 1/p and three orders in e [21]. Thus, the expectation is that the PN series there will be less extensive than what we are able to get from the redshift. Nevertheless, we should be able to extract some closed-form expressions, particularly at low orders, which will be fruitful as input for EOB models with spin.

Finally, with the PN behavior of the equatorial problem well understood, we will then be able to study the effects of inclination. EMRI behavior is greatly complicated by the  $\theta$  motion, particularly in the source integration. The authors of [94] were recently able to calculate the fluxes for generic EMRIs to  $5\text{PN}/e^{10}$ . It is expected that several of the computational simplifications applied here in the equatorial case will be applicable to generic orbits. In particular, the MST homogeneous solutions take identical forms in both

cases. Thus, we may have the opportunity to extend those results. The conservative sector will be more difficult still, as the metric perturbation expressions are significantly more cumbersome, and the *m* summation formulas derived for spheroidal harmonics in Sec. III relied on simplifications in the equatorial plane. Nevertheless, the potential remains to derive yet undiscovered closed-form PN terms at low orders. These possibilities will all be explored in future work.

#### ACKNOWLEDGMENTS

The author thanks Charles R. Evans, Jezreel Castillo, Scott Hughes, Zachary Nasipak, David Brown, Adrian Ottewill, Niels Warburton, Barry Wardell, and Chris Kavanagh for many helpful discussions in the preparation of this manuscript, and again thanks Zachary Nasipak for supplying the numerical redshift data. This work was supported by NSF Grants No. PHY-1806447 and No. PHY-2110335 to the University of North Carolina–Chapel Hill. This work was also supported by NASA ATP Grant No. 80NSSC18K1091 to the Massachusetts Institute of Technology. This work makes use of the black hole perturbation toolkit.

- [1] T. Hinderer and E. E. Flanagan, Phys. Rev. D **78**, 064028 (2008).
- [2] C. Munna, Eccentric-orbit binary black hole inspirals: Informing the post-Newtonian expansion through black hole perturbation theory and multipole moment analysis, Ph.D. thesis, University of North Carolina at Chapel Hill, 2020.
- [3] D. V. Gal'tsov, A. A. Matyukhin, and V. I. Petukhov, Phys. Lett. 77A, 387 (1980).
- [4] E. Poisson, Phys. Rev. D 47, 1497 (1993).
- [5] C. Cutler, L. S. Finn, E. Poisson, and G. J. Sussman, Phys. Rev. D 47, 1511 (1993).
- [6] H. Tagoshi and T. Nakamura, Phys. Rev. D 49, 4016 (1994).
- [7] M. Sasaki, Prog. Theor. Phys. 92, 17 (1994).
- [8] T. Tanaka, H. Tagoshi, and M. Sasaki, Prog. Theor. Phys. 96, 1087 (1996).
- [9] Y. Mino, M. Sasaki, M. Shibata, H. Tagoshi, and T. Tanaka, Prog. Theor. Phys. Suppl. **128**, 1 (1997).
- [10] R. Fujita, Prog. Theor. Phys. 128, 971 (2012).
- [11] T. Regge and J. Wheeler, Phys. Rev. 108, 1063 (1957).
- [12] F. Zerilli, Phys. Rev. D 2, 2141 (1970).
- [13] S. Mano, H. Suzuki, and E. Takasugi, Prog. Theor. Phys. 96, 549 (1996).
- [14] S. Mano, H. Suzuki, and E. Takasugi, Prog. Theor. Phys. 95, 1079 (1996).
- [15] C. Munna and C. R. Evans, Phys. Rev. D **100**, 104060 (2019).

- [16] C. Munna, C. R. Evans, S. Hopper, and E. Forseth, Phys. Rev. D 102, 024047 (2020).
- [17] C. Munna and C. R. Evans, Phys. Rev. D **102**, 104006 (2020).
- [18] C. Munna, Phys. Rev. D 102, 124001 (2020).
- [19] C. Munna, C. R. Evans, and E. Forseth, Phys. Rev. D 108, 044039 (2023).
- [20] C. Munna and C. R. Evans, Phys. Rev. D **106**, 044004
- [21] C. Munna and C. R. Evans, Phys. Rev. D **106**, 044058 (2022).
- [22] L. Barack, T. Damour, and N. Sago, Phys. Rev. D 82, 084036 (2010).
- [23] A. Le Tiec, L. Blanchet, and B. Whiting, Phys. Rev. D **85**, 064039 (2012).
- [24] D. Bini and T. Damour, Phys. Rev. D 90, 124037 (2014).
- [25] D. Bini, T. Damour, and A. Geralico, Phys. Rev. D 93, 064023 (2016).
- [26] A. Le Tiec, Phys. Rev. D 92, 084021 (2015).
- [27] S. Hopper, C. Kavanagh, and A. C. Ottewill, Phys. Rev. D 93, 044010 (2016).
- [28] C. Kavanagh, D. Bini, T. Damour, S. Hopper, A. Ottewil, and B. Wardell, Phys. Rev. D 96, 064012 (2017).
- [29] D. Bini, T. Damour, and A. Geralico, Phys. Rev. D 97, 104046 (2018).
- [30] D. Bini, T. Damour, and A. Geralico, Phys. Rev. Lett. **123**, 231104 (2019).

- [31] D. Bini, T. Damour, and A. Geralico, Phys. Rev. D 102, 024062 (2020).
- [32] D. Bini, T. Damour, and A. Geralico, Phys. Rev. D 102, 024061 (2020).
- [33] E. Poisson, Phys. Rev. D 48, 1860 (1993).
- [34] M. Shibata, M. Sasaki, H. Tagoshi, and T. Tanaka, Phys. Rev. D 51, 1646 (1995).
- [35] H. Tagoshi, Prog. Theor. Phys. 93, 307 (1995).
- [36] H. Tagoshi, M. Shibata, T. Tanaka, and M. Sasaki, Phys. Rev. D 54, 1439 (1996).
- [37] R. Fujita, Prog. Theor. Exp. Phys. 2015, 033E01 (2015).
- [38] S. Teukolsky, Astrophys. J. 185, 635 (1973).
- [39] M. Sasaki and H. Tagoshi, Living Rev. Relativity 6, 6 (2003).
- [40] C. Munna, J. Castillo, C. R. Evans, Z. Nasipak, and D. Brown (to be published).
- [41] C. Munna, J. Castillo, C. R. Evans, Z. Nasipak, and D. Brown (to be published).
- [42] S. Detweiler, Phys. Rev. D 77, 124026 (2008).
- [43] L. Blanchet, Living Rev. Relativity 17, 2 (2014).
- [44] D. Bini and T. Damour, Phys. Rev. D 87, 121501 (2013).
- [45] D. Bini and T. Damour, Phys. Rev. D 89, 064063 (2014).
- [46] C. Kavanagh, A. C. Ottewill, and B. Wardell, Phys. Rev. D 92, 084025 (2015).
- [47] L. Barack and N. Sago, Phys. Rev. D 83, 084023 (2011).
- [48] S. Akcay, A. Le Tiec, L. Barack, N. Sago, and N. Warburton, Phys. Rev. D 91, 124014 (2015).
- [49] A. G. Shah, J. L. Friedman, and T. S. Keidl, Phys. Rev. D 86, 084059 (2012).
- [50] D. Bini, T. Damour, and A. Geralico, Phys. Rev. D 92, 124058 (2015).
- [51] C. Kavanagh, A. C. Ottewill, and B. Wardell, Phys. Rev. D 93, 124038 (2016).
- [52] M. van de Meent and A. G. Shah, Phys. Rev. D 92, 064025 (2015).
- [53] D. Bini, T. Damour, and A. Geralico, Phys. Rev. D 93, 124058 (2016).
- [54] D. Bini and A. Geralico, Phys. Rev. D 100, 104002 (2019).
- [55] M. van de Meent, Classical Quantum Gravity 34, 124003 (2017).
- [56] P. L. Chrzanowski, Phys. Rev. D 11, 2042 (1975).
- [57] J. M. Cohen and L. S. Kegeles, Phys. Rev. D 10, 1070 (1974).
- [58] L. S. Kegeles and J. M. Cohen, Phys. Rev. D **19**, 1641 (1979).
- [59] R. M. Wald, Phys. Rev. Lett. 41, 203 (1978).
- [60] Black Hole Perturbation Toolkit, https://bhptoolkit.org/.
- [61] UNC Gravitational Physics Group, https://github.com/ UNC-Gravitational-Physics.
- [62] D. Bini, T. Damour, and A. Geralico, Phys. Rev. D 93, 064023 (2016).
- [63] C. Darwin, Proc. R. Soc. A 249, 180 (1959).
- [64] C. Cutler, D. Kennefick, and E. Poisson, Phys. Rev. D 50, 3816 (1994).
- [65] L. Barack and N. Sago, Phys. Rev. D 81, 084021 (2010).

- [66] D. Bini, A. Geralico, and R. T. Jantzen, Phys. Rev. D 94, 064066 (2016).
- [67] R. Fujita and W. Hikida, Classical Quantum Gravity 26, 135002 (2009).
- [68] C. O. Lousto and B. F. Whiting, Phys. Rev. D 66, 024026 (2002).
- [69] T. S. Keidl, A. G. Shah, J. L. Friedman, D.-H. Kim, and L. R. Price, Phys. Rev. D 82, 124012 (2010).
- [70] S. Chandrasekhar, The Mathematical Theory of Black Holes, The International Series of Monographs on Physics Vol. 69 (Clarendon, Oxford, 1983).
- [71] C. Merlin, A. Ori, L. Barack, A. Pound, and M. van de Meent, Phys. Rev. D 94, 104066 (2016).
- [72] E. Newman and R. Penrose, J. Math. Phys. (N.Y.) 3, 566 (1962).
- [73] H. Nakano, N. Sago, and M. Sasaki, Phys. Rev. D 68, 124003 (2003).
- [74] D. Bini and A. Geralico, arXiv:1908.03191.
- [75] S. R. Dolan, N. Warburton, A. I. Harte, A. Le Tiec, B. Wardell, and L. Barack, Phys. Rev. D 89, 064011 (2014).
- [76] S. Akcay, D. Dempsey, and S. Dolan, Classical Quantum Gravity 34, 084001 (2017).
- [77] S. L. Detweiler and B. F. Whiting, Phys. Rev. D 67, 024025 (2003).
- [78] A. Heffernan, A. Ottewill, and B. Wardell, Phys. Rev. D 86, 104023 (2012).
- [79] L. Barack, Phys. Rev. D 64, 084021 (2001).
- [80] L. Barack and A. Ori, Phys. Rev. D 67, 024029 (2003).
- [81] A. Pound, C. Merlin, and L. Barack, Phys. Rev. D 89, 024009 (2014).
- [82] S.L. Detweiler, Classical Quantum Gravity 22, S681 (2005).
- [83] T. Damour, P. Jaranowski, and G. Schäfer, Phys. Rev. D 91, 084024 (2015).
- [84] E. Forseth, C. R. Evans, and S. Hopper, Phys. Rev. D 93, 064058 (2016).
- [85] P. C. Peters and J. Mathews, Phys. Rev. 131, 435 (1963).
- [86] K. G. Arun, L. Blanchet, B. R. Iyer, and M. S. S. Qusailah, Phys. Rev. D 77, 064034 (2008).
- [87] K. G. Arun, L. Blanchet, B. R. Iyer, and M. S. S. Qusailah, Phys. Rev. D 77, 064035 (2008).
- [88] N. Loutrel and N. Yunes, Classical Quantum Gravity 34, 044003 (2017).
- [89] K. G. Arun, L. Blanchet, B. R. Iyer, and S. Sinha, Phys. Rev. D 80, 124018 (2009).
- [90] S. Isoyama, R. Fujita, H. Nakano, N. Sago, and T. Tanaka, Prog. Theor. Exp. Phys. **2013**, 063E01 (2013).
- [91] N. K. Johnson-McDaniel, Phys. Rev. D **90**, 024043 (2014).
- [92] Z. Zhang, N. Yunes, and E. Berti, Phys. Rev. D 84, 024029 (2011).
- [93] D. Bini, T. Damour, A. Geralico, C. Kavanagh, and M. van de Meent, Phys. Rev. D 98, 104062 (2018).
- [94] S. Isoyama, R. Fujita, A. J. K. Chua, H. Nakano, A. Pound, and N. Sago, Phys. Rev. Lett. 128, 231101 (2022).